Published in final edited form as:
Dev Biol. 2014 January 15; 385(2): 380–395. doi:10.1016/j.ydbio.2013.11.011.

Evolution of a developmental mechanism: species-specific regulation of the cell cycle and the timing of events during craniofacial osteogenesis

Jane Hall[*], **Andrew H. Jheon**[*], **Erin L. Ealba**, **B. Frank Eames**, **Kristin D. Butcher**, **Siu-Shan Mak**[†], **Raj Ladher**[†], **Tamara Alliston**, and **Richard A. Schneider**[‡]

Abstract

Neural crest mesenchyme (NCM) controls species-specific pattern in the craniofacial skeleton but how this cell population accomplishes such a complex task remains unclear. To elucidate mechanisms through which NCM directs skeletal development and evolution, we made chimeras from quail and duck embryos, which differ markedly in their craniofacial morphology and maturation rates. We show that quail NCM, when transplanted into duck, maintains its faster timetable for development and autonomously executes molecular and cellular programs for the induction, differentiation, and mineralization of bone, including premature expression of osteogenic genes such as *Runx2* and *Col1a1*. In contrast, the duck host systemic environment appears to be relatively permissive and supports osteogenesis independently by providing circulating minerals and a vascular network. Further experiments reveal that NCM establishes the timing of osteogenesis by regulating cell cycle progression in a stage- and species-specific manner. Altering the time-course of D-type cyclin expression mimics chimeras by accelerating expression of *Runx2* and *Col1a1*. We also discover higher endogenous expression of *Runx2* in quail coincident with their smaller craniofacial skeletons, and by prematurely over-expressing *Runx2* in chick embryos we reduce the overall size of the craniofacial skeleton. Thus, our work suggests that NCM establishes species-specific size in the craniofacial skeleton by controlling cell cycle, *Runx2* expression, and the timing of key events during osteogenesis.

Keywords

Cranial neural crest; craniofacial osteogenesis; cell cycle regulation; Runx2; quail-duck and quail-emu chimeras; evolutionary developmental biology

INTRODUCTION

The avian craniofacial skeleton exemplifies one of the most highly diversified and adapted anatomical structures across vertebrates. Its size and shape can change rapidly and its overall structure can reflect ecological and functional demands with remarkable precision, as famously represented by the beaks of Darwin's finches. Understanding how the craniofacial

[‡]**Corresponding author address:** University of California at San Francisco, Department of Orthopaedic Surgery, 513 Parnassus Avenue, S-1164, San Francisco, CA 94143-0514, rich.schneider@ucsf.edu.
[*]These authors contributed equally to this work
[†]**Author affiliation:** RIKEN Center for Developmental Biology, 2-2-3 Minatojima-minami, Chuo-ku Kobe, Japan 650-0047

AUTHOR CONTRIBUTIONS

R.A.S. conceived the project; R.A.S., B.F.E., A.H.J., J.H., E.L.E., K.D.B., and S.S.M. performed the experiments; R.A.S., A.H.J., J.H., and E.L.E. compiled the data; R.A.S., A.H.J., J.H., and E.L.E., R.L., and T.A. designed the experiments and analyzed the data; and J.H., A.H.J., and R.A.S. co-wrote the manuscript.

skeleton becomes modified through evolution requires insights on where and when species-specific changes to the osteogenic program arise during development. To this end, we employ a unique avian chimeric transplantation system that takes advantage of the divergent maturation rates and distinct species-specific beak anatomies of quail and duck. We experimentally manipulate neural crest mesenchyme (NCM), an embryonic cell population that migrates out of the midbrain and rostral hindbrain and forms all of the bones in the beak skeleton. Previously, we have shown that NCM, when transplanted between quail and duck autonomously controls the species-specific patterning of the face, and produces short quail-like beaks on duck hosts ("quck") and long duck-like bills on quail hosts ("duail") (Jheon and Schneider, 2009; Lwigale and Schneider, 2008; Schneider, 2005, 2007; Schneider and Helms, 2003). Further investigations have uncovered mechanisms through which NCM exerts its species-specific effects on the cartilaginous skeleton (Eames and Schneider, 2008), the epidermis (Eames and Schneider, 2005), the jaw musculature and adjacent connective tissues (Solem et al., 2011; Tokita and Schneider, 2009), and the overlying epithelium during intramembranous ossification (Merrill et al., 2008), but little is known about mechanisms through which NCM directs species-specific formation of the bony skeleton.

Osteogenesis is a complex process involving numerous genes, cells, tissues, signaling interactions, and hierarchical levels of control. Here, we report that NCM exerts intrinsic control over the timing of key osteogenic events, including expression of the osteogenic transcription factor *Runx2*. We further confirm that NCM plays a dominant and species-specific role during osteogenesis by performing quail-emu transplants where the alteration of events is even more dramatic and extreme. We propose that this programmatic integration on the molecular, cellular, and histological levels serves as a mechanism that enables NCM to transmit species-specific size to bones in the craniofacial skeleton.

To identify mechanisms through which NCM exerts its effects on osteogenesis we focus on regulation of the cell cycle. Many *in vitro* studies have shown that osteoblast differentiation is tied to cell cycle exit (Drissi et al., 1999; Galindo et al., 2005; Pratap et al., 2003; Thomas et al., 2004; Young et al., 2007). Here we demonstrate that NCM controls cell cycle progression *in vivo*. We analyze expression of cyclins and cyclin-dependent kinase inhibitors (CKIs) such as p27 (*Cdkn1b*), cyclin E (*Ccne1*), cyclin B1 (*Ccnb1*), and cyclin D1 (*Ccnd1*) in quail, duck, and quck chimeras, and find both stage-specific and species-specific regulation. Then, by experimentally altering the time-course during which D-type cyclins are expressed prior to osteogenesis, we are able to phenocopy the quck chimera in so far as accelerating the onset of *Runx2* and *Col1a1* expression. Lastly, we identify differences between quail and duck in their endogenous levels of *Runx2* expression, and show that by over-expressing *Runx2* prematurely, we are able to reduce the size of the craniofacial skeleton. Taken together, these data reveal that NCM dictates when bone forms by controlling the timing of cell cycle progression and mediating the transition from cell proliferation to differentiation. Moreover, our data show that *in vivo* mechanisms regulating the cell cycle can directly affect *Runx2* expression, and this expression not only varies between species, but also ultimately influences the size of bone. Thus, this work offers a developmental mechanism through which NCM can direct the evolution of the craniofacial skeleton.

MATERIALS AND METHODS

Generation of chimeras

Eggs from Japanese quail (*Coturnix coturnix japonica*), white Pekin duck (*Anas platyrhynchos*) (AA Labs, Westminster, CA), and Australian emu (*Dromaius novaehollandiae*) were incubated at 37°C until reaching HH9.5 (Figure 1B). Embryos were handled following University and NIH guidelines. Tungsten needles and Spemann pipettes

were used for operations (Schneider, 1999). Unilateral and bilateral grafts of rostral hindbrain and midbrain neural crest were excised from quail donors and transplanted into either stage-matched duck hosts, producing chimeric 'quck' (Schneider and Helms, 2003) or emu, producing chimeric "qumu." Equivalent transplants were also made from duck to quail ('duail'). Donor tissue was inserted into a host that had comparable regions of tissue removed (Figure 1C). Control orthotopic grafts and sham operations were made within each species. Controls were incubated alongside chimeras to ensure that stages of grafted cells were accurately assessed. In addition, unilateral transplants provided an internal control on the un-operated host side.

Histology and immunohistochemistry

Tissues were collected in Serra's fixative overnight at 4°C, dehydrated, paraffin embedded, and cut into 7 μm frontal sections. Section were stained with Milligan's Trichrome (Presnell and Schreibman, 1997) or immunostained with the Q¢PN (quail-specific) antibody (Developmental Studies Hybridoma Bank, University of Iowa) as described (Schneider, 1999).

Whole-mount embryo staining

For skeletal analyses, embryos were fixed in 4% paraformaldehyde (PFA) overnight, stained with Alcian blue and/or Alizarin red, and cleared in glycerol as described (Wassersug, 1976). For analyses of alkaline phosphatase activity, embryos were fixed in 4% PFA for 20 min at 4°C, and stained using 4-nitro blue tetrazolium chloride (NBT; Roche) and 5-bromo-4-chloro-3-indolyl-phosphate (BCIP; Roche) as described (Liu et al., 1999)

Gene expression analysis

In situ hybridization analyses were performed as described (Albrecht et al., 1997). Briefly, sections were hybridized overnight with ^{35}S-labeled chick riboprobes generated from plasmids containing chicken collagen type Iα (*Col1a1*), *Runx2*, tissue non-specific alkaline phosphatase (*Tnap*), bone sialoprotein (*Bsp*), osteopontin (*Opn*), vascular endothelial growth factor (*Vegf*), fetal Liver Kinase 1 (Flk1), and RSV viral envelope (*Env*). Reverse transcription quantitative real-time PCR (RT-qPCR) analyses were performed on total RNA (isolated from embryonic mandibles of quail, duck, and bilaterally transplanted quck (RNeasy, Qiagen). cDNA was generated using the iScript cDNA synthesis kit (BioRad) and RT-qPCR was performed in triplicates using the iScript SYBR Green RT-PCR kit (Biorad) on an iQ5 cycler (Biorad). Primers were generated using NCBI Primer-BLAST software for the following chicken genes: *Col1a1* (Forward 5'- CCCGACCCTAAGACAAAGAG -3'; Reverse 5'- GCTACTTACTGTCCTCTTCTCC - 3'), *Runx2* (Forward 5' - TGGACCTTTCCAGACCAGCAGCA - 3'; Reverse 5' - GGCAAGTTTGGGTTTAGCAGCGT - 3'), p27 (Forward 5'- TTCGGCCTACACAGTGAGTG -3'; Reverse 5'- CGATTTCTTGGGTGTTTGCT - 3'), avian *cyclin D1* (Forward 5' - CTTGGATGCTGGAGGTCTGC - 3'; Reverse 5' - CTGCGGTCAGAGGAATCGTT - 3'), mouse *cyclin D1* (Forward 5' - TGAGGAGCAGAAGTGCGAAG- 3'; Reverse 5' - AGATGCACAACTTCTCGGCA- 3'), and *eGFP* (Forward 5′ - GCAGAAGAACGGCATCAAGGT - 3′; Reverse 5′ - ACGAACTCCAGCAGGACCATG - 3′). Gene expression was normalized to the expression of the RPL19 (Forward 5'- ACGCCAACTCGCGTCAGCAG - 3'; Reverse 5'- ATATGCCTGCCCTTCCGGCG - 3'), and fold changes were calculated using the delta-delta C(t) method (Livak and Schmittgen, 2001).

Proliferation analysis

One μL of BrdU (Invitrogen, Carlsbad, CA) was injected into an intravitelline vein and chimeric and control embryos were incubated for 20 min at 37°C (Schneider et al., 2001). Embryos were fixed in Serra's solution, sectioned, and stained using a BrdU staining kit (Invitrogen). Chimeric quck embryos were screened (using Q¢PN) for those cases that had a large majority of quail donor-derived NCM on one side of the mandible and no contamination from the donor on the contralateral host side. Sections adjacent to these screened cases were used to quantify BrdU-positive cells using ImageJ software (NIH). The rectangular selection tool was used to define equal areas on donor and host sides of quck through a depth of 0.5 – 0.9 mm (average volume of 0.06 – 0.1 mm^3). Relative levels of BrdU-positive cells were compared between the donor and host sides in quck (n = 9).

Flow cytometry

Dissociated NCM from mandibular primordia of quail, duck, and bilaterally transplanted quck were fixed in 70% ethanol and stained with 1 mg/mL propidium iodide (Invitrogen), 2 μg RNAse (Roche), and 0.1% Triton X-100 for 15 min at 37°C. Flow cytometry was performed using a Cytomation MoFlo High Speed Sorter to detect propidium iodide and cell cycle phases were estimated using the Watson model analyses in the FlowJo software (Ver. 7.2.2).

Serum calcium and phosphorus levels

Blood (20–100 μL) was collected from duck and quck embryos via a glass needle inserted into the vitelline vein. Blood serum was isolated by incubating for 1h at 37°C, followed by centrifugation (700×g, 10 min). Calcium and phosphorus levels in collected or commercially available control serum (DC-Trol, Diagnostic Chemicals Ltd., Charlottetown, PEI) were measured in a Spectra Max M5 multi-well plate reader (Molecular Devices, Sunnyvale, CA) using the Calcium and Phosphorus Assay kit following the manufacturer's protocol (Diagnostic Chemicals Ltd.).

Analyses of vascularization

Using glass needles (diameter 0.5 mm, Sutter Instruments Co.), 5 μL of FluoSphere carboxylate-modified microspheres (0.2u, 580/605; Invitrogen) or rhodamine-conjugated *Lens culinaris* agglutinin (Vector Laboratories, Inc.) were injected into the vitelline vein of quck chimeras using a PV830 Pneumatic Picopump (World Precision Instruments, Sarasota, FL). Fifteen minutes after injection, embryos were fixed in 4% PFA overnight. For FluoSphere-injected embryos, mandibles were dissected, cleared in glycerin, and imaged using epifluorescence (Leica MZFLIII stereoscope). For quantification, relative fluorescent units (RFU) were measured on the donor versus host sides using a Spectra Max M5 multi-well plate reader. For lectin-injected embryos, embryos were incubated in 5–30% sucrose/PBS overnight, embedded in tissue freezing media (Triangle Biomedical Sciences, Durham, N.C.), and cryosectioned (20 μm). Sections were stained with Q¢PN and Alexa Fluor 488 goat anti-mouse IgG (Invitrogen) secondary antibody, and Hoescht reagent. Quantification of blood vessels was performed as described above for quantifying BrdU-positive cells.

Western Blot

Mandibles from HH24-HH30 control embryos and HH27 chimeric embryos were syringe-lysed with a 22½G needle in 1X RIPA Buffer with cOmplete, Mini Protease Inhibitor Cocktail (Roche) and 0.5 mM phenylmethylsulfonyl fluoride (PMSF). Proteins were separated on 10% SDS-polyacrylamide gels, transferred onto nitrocellulose membranes at 300mA for 1.5 hours, blocked in 5% milk, and detected with the appropriate primary antibody. Primary antibodies used were against β-actin (Abcam ab8229), cyclin E (Santa

Cruz M-20), cyclin B1 (Santa Cruz H-433), p27 (BD Biosciences BD610241), and cyclin D1/D2 (Santa Cruz, C-17). Appropriate secondary was applied prior to imaging. Secondary antibodies used were Alexa Fluor 488 goat anti-mouse (Invitrogen), goat anti-mouse IRDye 800CW (LICOR), and goat anti-rabbit IRDye 680LT (LICOR). Antibody-bound proteins were visualized using a LICOR Odyssey Infrared Imager, and quantifications were performed using LICOR Odyssey software.

Electroporation

In ovo electroporation was performed using a 1:1 solution of 2 μg/μl pCIG-cyclinD1-IRES-eGFP and pCIG-cyclinD2-IRES-eGFP constructs (a gift from F. Pituello, described in Lobjois, et al. 2004, 2008). With the addition of Fast Green tracer dye, DNA solution was injected into HH8 quail neural tubes with pulled glass micropipettes and a Picospritzer fluid injector. Platinum electrodes were positioned on each side of the area pellucida, centered on the midbrain-hindbrain boundary, and a IntraCel TSS20 Ovodyne Electroporator was used to administer three square, 50-ms long, 10 volt pulses, with 50 ms spaces, to allow unilateral entry of the DNA into the neural crest mesenchyme, with the contralateral (un-electroporated) side serving as the control. Electroporation efficiency was evaluated at embryo collection by epiflourescent imaging of eGFP expression.

Retroviral Expression

The RCAS-Runx2 construct was a gift from S. Mundlos (Stricker et al., 2002). RCAS virus was produced as described (Morgan and Fekete, 1996). DF-1 cells were acquired from the American Type Culture Collection (Manassus, VA). Fast Green tracer dye and DNA solution was injected into HH8 neural tubes of virus-free SPAFAS chick (Charles River Labs) using pulled glass micropipettes and a Picospritzer fluid injector. Control SPAFAS chick embryos were injected with RCAS-GFP (Chen et al., 1999).

Statistical methods

Unpaired Student's t-tests were used for comparisons of continuous variables between exactly two groups. Two-tailed $p<0.05$ was considered statistically significant, and $p<0.01$ was considered very statistically significant.

RESULTS

NCM establishes the timing of craniofacial mineralization

To understand the role that NCM plays during the formation of bone in the craniofacial skeleton we transplanted first arch (i.e., mandibular) neural crest cells from quail to duck, and produced chimeric quck. Quail and duck not only display species-specific differences in their beak size and shape (Figure 1A), but they also develop at highly divergent rates (Figure 1B). The unilateral transplantation of mid- and hindbrain neural crest cells from quail to duck (Figure 1C) leads to the formation of quail-derived beak components on one side of the embryo (Figure 1E, F), which are quail-like in their size and shape (Eames and Schneider, 2008; Schneider and Helms, 2003). By design, the host side serves as an internal control and the distribution of quail cells can be followed using an antibody (Q¢PN) that binds to cells from the quail but not from the duck (Figure 1D).

To determine the extent to which NCM governs the timing of osteogenesis, we analyzed the onset and progression of mineralization in quail, duck, and quck by whole-mount Alizarin red staining (Hanken and Wassersug, 1981; Wassersug, 1976). The first evidence of any mineralization was observed in the distal tibia of quail and duck at HH33 (data not shown), but there was no Alizarin red staining anywhere in the head skeleton of quail or duck

(Figure 2A and data not shown), which is consistent with previous observations in chick and other avian species (Mitgutsch et al., 2011; Pechak et al., 1986). The bones of the craniofacial skeleton of quail and duck showed their first signs of mineralization at HH34 (Fig 2C, D). In quck however, the initiation of craniofacial mineralization on the quail donor side occurred three stages earlier at HH31 (Figure 2B), long before the onset of tibial mineralization at HH33. Moreover, the extent of mineralization on the quail donor side of quck at HH34 and HH36 (Figure 2E, H) was like that of quail at HH37 and HH39 (Figure 2F, I), respectively. The host side of quck was always similar to that observed in the stage-matched duck control (Figure 2D, G). Conversely, in reciprocal transplants producing duail chimeras, the presence of duck donor-derived NCM (i.e., Q¢PN-negative cells; Figure 2J) delayed craniofacial mineralization in quail hosts by three stages. Initially the duck donor side remained unmineralized while the faster-developing quail host side started to mineralize (Figure 2K). In later-staged quail hosts, the duck donor side maintained its slower progression but eventually mineralized (Figure 2L). Thus, relative to the stage of the local environment, NCM can either speed up or slow down the timing of mineralization depending on its species-specific rate of development.

NCM regulates the expression of genes involved in mineralization

To determine if quail donor NCM accelerates mineralization by regulating genes known to play a role during mineralization, we performed *in situ* hybridization on tissues from quail, duck, and quck. We focused on the angular bone adjacent to the mandibular (i.e., Meckel's) cartilage, since this is one of the earliest elements to mineralize in the head (Figure 3A, D). In HH32 duck, quail (data not shown), and the host side of stage-matched quck, we observed little or no expression of mineralization factors such as tissue non-specific alkaline phosphatase (*Tnap*) (Figure 3E, F), bone sialoprotein (*Bsp*) (Figure 3I, J), and osteopontin (*Opn*) (Figure 3M, N). However, on the quail donor side of quck, *Tnap, Bsp*, and *Opn* were all highly expressed (Figure 3G, K, O), coincident with the presence of quail donor NCM (Figure 3C) and equivalent to that observed in HH35 quail (Figure 3H, L, P). Thus, NCM controls the timing of expression of genes that play a role in matrix mineralization.

Host blood mineral levels are not regulated by donor NCM

To assess whether the ability of chimeras to mineralize prematurely was due to donor-mediated effects on systemic (i.e., host) levels of circulating minerals required for mineralization, we measured serum calcium and phosphorus levels in duck and quck at time points ranging from HH28 to HH38 (Figure 3Q). Duck calcium levels were relatively constant between HH28 to HH38, whereas phosphorus levels increased significantly between HH28 and HH31 ($p=0.0001$), and decreased thereafter. Similar results were obtained in quck between HH28 and HH31 ($p=0.01$; Figure 3Q) and thus, we observed no donor-specific effects on host blood mineral levels.

Neural crest mesenchyme controls the timing of osteoid deposition

To evaluate the ability of NCM to govern osteogenic events prior to mineralization, we compared the deposition of extracellular matrix (i.e., osteoid) in quail, duck, and quck beaks. Osteoid was present in the beaks of quail (Figure 4D, H) and duck (data not shown) at HH34, but not at HH31 (Figure 4A, E). In quck, osteoid was visible three HH stages earlier on the quail donor side at HH31 (Figure 4C, G) coincident with Q¢PN-positive staining (Figure 4K), but not on the duck host side (Figure 4B,F).

To test the capacity of NCM to direct osteogenesis even further and to understand how permissive the host environment might be, we created chimeras using another avian species with a much more divergent maturation rate and facial morphology, which is the Australian emu. Emu take around 50 days to hatch, versus 28 days in duck, and 17 days in quail. We

transplanted quail NCM into emu and in resulting “qumu” we found that donor quail NCM was able to undergo osteogenesis at a vastly accelerated rate relative to the very slow-developing emu host. At HH27, when the internal control side of the emu mandibular arch was composed mainly of host mesenchyme just beginning to undergo cartilage matrix deposition and preosteogenic condensation, the quail donor side showed a fully developed mandibular cartilage and robust osteoid deposition, representing an acceleration of about seven HH stages (Figure 4M, N), which is more than twice the difference observed in quck.

NCM controls the timing of osteoblast differentiation

To investigate the ability of NCM to regulate the timing of osteoblast differentiation, we assayed for the enzymatic activity of alkaline phosphatase (Ishii et al., 2003) in the beak primordia. Low levels of alkaline phosphatase activity were detected in HH26 duck (Figure 5A) and quail (data not shown), and much higher levels at HH29 (Figure 5C and data not shown). The quail donor side of HH26 quck showed high levels of alkaline phosphatase activity as determined by darker staining relative to the duck host side like that observed in HH29 quail (Figure 5B). We then analyzed the extent to which NCM modulates the expression of genes required for osteoblast differentiation by *in situ* hybridization and RT-qPCR. Expression levels for the osteogenic genes collagen type 1 (*Col1a1*) and *Runx2* were substantially higher on the quail donor side in HH24 quck (Figure 5D, F). *In situ* hybridization data were supported by RT-qPCR data that showed a significant up-regulation of *Col1a1* and *Runx2* between HH24 and HH27 in both quail and duck, whereas this up-regulation was observed three stages earlier in quck between HH21 and HH24 (Figure 5E, G).

Donor NCM does not affect the timing of host blood vessel formation

Given the ability of NCM to accelerate the timing of osteogenesis and the reliance of bone formation on the process of vascular invasion (Gerber et al., 1999; Thompson et al., 1989), we also assessed if donor NCM might be prematurely recruiting a blood supply in the host. Specifically, we examined the extent of host blood vessel formation by labeling the vasculature of HH24 quck, which is an embryonic stage when small vessels are present in the mandibular arch (Noden, 1989, 1990). We triple-stained tissue sections with *Lens Culinaris* Agglutinin for blood vessels, Q¢PN for donor NCM, and Hoescht dye for all cells (Figure 5H) and then quantified total vasculature over a fixed volume (Figure 5J). Surprisingly, we observed no difference between quail donor and host sides in HH24 quck. In a separate series of experiments designed to measure vasculature in whole mandibles, we filled the host bloodstream with fluorescent microspheres (Figure 5I). Fluorescence as a measure of vessel volume was quantified, and again, no differences were detected in the amount of vasculature between quail donor and host sides in HH24 quck (Figure 5K). Lastly, *in situ* hybridization for two markers of developing vasculature, *Vegf* and its receptor, *Flk1*, was performed on sections from HH24 quck. Unlike what we had observed for osteogenic genes, we did not detect any differences in the timing or levels of expression for these angiogenic markers between quail donor and host sides (data not shown). Thus, NCM does not affect the timing or extent of blood vessel formation during early stages of osteogenesis, rather the angiogenic program appears to be executed independently by non-neural crest-derived tissues in the host environment.

NCM regulates cell cycle progression

After finding that NCM controls osteogenic differentiation and subsequent mineralization, we wanted to investigate if this ability arises due to NCM also mediating the critical transition from proliferation to differentiation that occurs during early stages of osteogenic induction. We used two approaches. First, the extent of cell division was measured by BrdU

incorporation in those HH24 quck mandibles containing large numbers of quail donor NCM (Figure 6A). Anti-BrdU staining showed less BrdU incorporation on the quail donor side relative to the duck host side, suggesting a premature decrease in proliferation (Figure 6B). Quantitative measurements confirmed an approximately 40% reduction in the number of proliferating cells on quail donor side relative to duck host side in the same volume of mandible in quck ($p=0.013$) (Figure 6C). Second, we examined progression through the cell cycle from HH21 to HH27 in quail, duck, and quck via propidium iodide staining (to label all DNA), and subsequent flow cytometry (FACS). To ascertain the ability of NCM to control progression past the G1/S checkpoint, we quantified the percentage of cells in G1 phase, versus the percentage of those in S and G2/M phases. In quail and duck, there was a significant increase in G1-phase cells, along with the expected reciprocal decrease in S+G2/M-phase cells between HH24 and HH27 ($p=0.049$ (quail), $p=0.003$ (duck)), which spans the time when cells in the mandible transition from proliferation to differentiation. In quck, the increase in G1-phase cells occurred three stages earlier, between HH21 and HH24, as did the reciprocal decrease in S+G2/M-phase cells (Figure 6D and data not shown; $p=0.029$). Thus, NCM controls the timing of the transition from proliferation to differentiation that enables osteogenesis to proceed.

NCM modulates levels of cell cycle regulators

Given that NCM establishes its own time course for exiting the cell cycle, we sought to identify mechanisms by which NCM could accomplish this task and therefore analyzed cyclin and cyclin-dependent kinase inhibitor (CKI) protein expression in the mandibular mesenchyme of quail, duck, and quck from HH24 to HH30. In particular, we examined p27 (*Cdkn1b*), which is a CKI that decreases proliferation in a range of cell types including differentiating osteoblasts; cyclin E (*Ccne1*), which is required for G1/S phase transition; and cyclin B1 (*Ccnb1*), which is required for G2/M phase transition (Coats et al., 1996; Drissi et al., 1999; Zavitz and Zipursky, 1997).

From these analyses, we discovered stage-, species-, and/or tissue-specific patterns of gene and protein expression. Expression of p27 mRNA increased between HH21 and HH27 in both quail and duck (Figure 6E), yet p27 protein expression remained relatively constant in duck, and rose only marginally in quail from HH24 to HH30 (Figure 6F, G). We also observed that a single isoform of p27 protein predominated in the mandible at the time points studied, in contrast to the two isoforms detected in the frontonasal processes of chicken and duck at HH17 to HH31, as presented in a recent report (Powder et al., 2012). cyclin E protein expression decreased in control duck ($p=0.005$, HH24 to HH27; $p=0.007$, HH27 to HH30). However, at all stages studied in quail, we detected almost no intact cyclin E protein (Figure 6G), and instead we observed a large smear at a higher molecular weight like that resulting from post-translational modification of cyclin E that leads to its degradation (Doronkin et al., 2003). Protein levels of cyclin B1 decreased from HH24-HH30 in control quail and duck (Figure 6H), although this decrease occurred earlier in quail ($p=0.017$, HH24 to HH27; $p=0.038$, HH27 to HH30) than in duck (no statistically significant decrease HH24 to HH27; $p=0.030$, HH27 to HH30).

In chimeric quck mandibles collected at HH27, gene expression as well as levels and patterns of protein expression were altered on the quail donor side relative to the duck host side, and resembled that found in control quail three stages later. We observed quail donor-mediated changes to p27 gene expression (Figure 6E), but as in control quail and duck (Figure 6F), we did not detect differences at the p27 protein level (Figure 6J). However, we did observe statistically significant differences in protein levels analyzed from the donor versus host side for cyclin E ($p=0.0001$) and cyclin B1 ($p=0.041$). Expression patterns for both proteins were more like that observed in HH30 quail than in duck (Figure 6K, L). In the

case of cyclin E protein, we also observed a post-translational modification pattern on the donor side that was partly quail and partly duck (Figure 6K), likely as a consequence of samples containing tissues derived from both the donor (i.e., NCM) and the host (e.g., mandibular epithelium, myoblasts, and angioblasts/vascular endothelium). Thus, NCM likely regulates cell cycle through stage- and species-specific expression of cyclins and CKIs.

Altering levels of D-type cyclins can accelerate markers of osteogenesis

To test if osteogenic differentiation and cell cycle progression are mechanistically connected within NCM, we attempted to modify the stage at which NCM transitions from proliferation to differentiation by transiently over-expressing D-type cyclins. D-type cyclins promote proliferation, and over-expression has been sufficient to alter the timing of differentiation or cell fates in other systems (Lobjois et al., 2004). We first analyzed endogenous cyclin D1 protein expression from HH24-HH30, which spans the onset of osteoblast differentiation. Like the stable expression of p27 protein observed during these stages (Figure 6F), we found that endogenous quail cyclin D1 protein levels were also relatively constant (Figure 7A). We electroporated a combination of two bicistronic constructs containing mouse cyclin D1 plus enhanced Green Fluorescent Protein (eGFP), and mouse cyclin D2 plus eGFP, into the presumptive NCM of HH8 quail. This resulted in the transient over-expression of these genes throughout early development until HH18. Thereafter, we determined that the exogenous (i.e., mouse) cyclin D1 levels were decreased to endogenous (i.e., quail) levels by HH24. This phenomenon was likely due to the normal rate of dilution for this type of electroporated construct (Swartz et al., 2001) and thus, high eGFP expression was observed visually at HH18, much less at HH21, and not at all by HH24 (Figure 7B, C, and data not shown). this experimental design enabled us to generate an artificial transition from elevated to decreased levels of cyclin D1/D2 by HH24, which is the same stage at which we observed the accelerated transition from proliferation to differentiation in chimeric quck and premature expression of *Runx2*. Similarly, in our electroporated embryos collected at HH24, we found that the premature decrease in exogenous cyclin D1/D2 expression correlated with large and premature increases in *Runx2* (5-fold) and *Col1a1* (3-fold) expression at a stage when these genes are normally expressed at low levels (Figure 7D). In contrast, *Runx2* and *Col1a1* were only expressed at low levels while exogenous cyclin D1/D2 expression was high at HH18 (Figure 7D). Therefore, by artificially elevating and then decreasing D-type cyclin levels before osteogenesis would normally occur, we were able to drive early up-regulation of *Runx2* and *Col1a1*, and mimic the effects of quail donor NCM in a duck host, which also showed a 5-fold increase for *Runx2* and a 3-fold increase for *Col1a1* (Figure 5E and 5G).

Timing and levels of Runx2 expression affect beak size

To understand the consequences of premature *Runx2* up-regulation, as observed in our chimeric transplant and cyclin D1/D2 over-expression experiments, we used an avian retrovirus (RCAS) to over-express *Runx2* (or GFP in controls) continuously in the beak primordia of chick embryos. We infected embryos at HH8 (either bilaterally or unilaterally), and thus, with this experimental design, *Runx2* was expressed earlier and at higher levels than normal. *Runx2* over-expression was confirmed by *in situ* hybridization for a viral envelope gene (*Env)* and *Runx2* (Figure 7E, F), and RCAS-GFP infection was confirmed visually by epifluorescent microscopy (data not shown). After collecting treated embryos at HH38 and evaluating gross morphology and Alizarin red staining, we observed a dramatic decrease in the size of the beak skeleton (Figure 7G and H). By examining earlier stages in development, we found this effect on size was already apparent by HH26 (data not shown).

After demonstrating a relationship between *Runx2* expression levels and beak size, we investigated whether endogenous levels of *Runx2* expression differ between the small-beaked quail and the large-billed duck. When examining stages prior to the overt differentiation of bone in the mandible (HH24-HH32), we found no statistically significant differences in the levels of *Runx2* expression between quail and duck (Figure 7I). However, by the time osteogenesis progressed to include matrix deposition and mineralization (HH36-HH38), quail *Runx2* levels were more than double that of duck ($p=0.014$). Thus, based on these observations and our experimental data, NCM likely employs *Runx2* as a molecular mechanism to affect the size of the beak skeleton.

DISCUSSION

Timing of osteogenesis is a key mechanism in the evolution of skeletal size

An understanding of how birds have achieved such tremendous evolutionary variation in their craniofacial skeletons has come about gradually through a variety of experimental approaches. Fate-mapping studies first revealed that all of the skeletal elements of the jaws and face are derived from NCM (Cerny et al., 2004; Couly et al., 1993; Köntges and Lumsden, 1996; Le Lièvre and Le Douarin, 1975; Noden, 1978; Noden and Schneider, 2006; Schneider et al., 2001). Transplant experiments then demonstrated that NCM is the source of species-specific patterning information that not only regulates the growth of its own derivatives, but also that of surrounding structures (Eames and Schneider, 2005, 2008; Merrill et al., 2008; Schneider and Helms, 2003; Solem et al., 2011; Tokita and Schneider, 2009; Tucker and Lumsden, 2004). Additionally, other work has shown that NCM relies upon and is highly responsive to signals in the local environment that affect gene expression and also provide input on the axial orientation, identity, size, and shape of the beak skeleton (Abzhanov et al., 2006; Abzhanov et al., 2004; Barlow et al., 1999; Barlow and Francis-West, 1997; Couly et al., 2002; Foppiano et al., 2007; Francis-West et al., 1998; Francis-West et al., 1994; Hu and Marcucio, 2009a, b, 2012; Hu et al., 2003; Jeong et al., 2004; Shigetani et al., 2000; Wedden, 1987; Wu et al., 2006; Wu et al., 2004). But what has remained elusive are the precise molecular and cellular mechanisms through which NCM carries out what is undoubtedly a very complex task, which is providing species-specific patterning information to the craniofacial skeleton with great precision for proper function in established niches, but also with maximal plasticity for evolution in response to fluctuations in the natural environment.

Our results suggest that NCM provides species-specific patterning information to the craniofacial skeleton, especially in relation to size, by controlling the timing of key events during bone formation. Following transplantation, quail donor NCM maintains its faster timetable for development within the slower environment of the duck host and autonomously executes molecular and cellular programs for each step of osteogenesis, from induction to mineralization. This capacity holds true both in reverse and in the extreme, as evidenced by chimeric duail and qumu, respectively. Thus, NCM functions as the timekeeper that determines when osteogenesis begins during development. Moreover, we show that the temporal control that NCM exerts over this process appears closely tied to its ability to regulate cell cycle progression in a stage- and species-specific manner. Ultimately, this mechanistic link between cell cycle and osteogenesis may empower NCM with the ability to generate changes in skeletal size during evolution.

The ability of NCM to exert its effects on osteogenesis occurs at the population level and notably, the number of transplanted cells does have varying effects on the penetrance of the chimeric phenotype (Lwigale and Schneider, 2008). Chimeric embryos used in our study likely contained greater than 60% of transplanted cells in the region of interest, and this percentage was determined empirically by screening chimeric cases using a variety of

criteria (Ealba and Schneider, 2013). However, we also find that small populations of transplanted quail donor cells can give rise to isolated pockets of prematurely elevated *Runx2* expression that coincides with lower BrdU staining (data not shown). This phenomenon further demonstrates that cell cycle progression, *Runx2* expression, and ultimately, osteogenesis are controlled cell-autonomously within the NCM.

The local and systemic environments play a permissive role during osteogenesis

Craniofacial bones are highly vascularized and blood vessels infuse essential systemic components. The process of vascular invasion during intramembranous ossification has seldom been addressed experimentally (Thompson et al., 1989). Pericytes, which are derived from NCM, participate in the genesis and maintenance of blood vessels by providing smooth muscle, by responding to angiogenic factors, by modulating vascular permeability, and by guiding vasculogenesis (Bergers and Song, 2005; Betsholtz et al., 2005; Chantrain et al., 2006). Little is known about mechanisms through which osteogenic mesenchyme, pericytes, and vascular endothelium interact.

Part of our study was designed to address the capacity of NCM to regulate the timing of vascular invasion. In other words, we asked does quail NCM recruit a premature blood supply in duck hosts? We conclude that the donor NCM does not accelerate the timing or extent of blood vessel formation. However since we simply quantified volume, our analyses do not allow us to make a determination as to whether the vasculature shows a species-specific pattern. Thus, we cannot rule out the possibility that there are spatial differences in the organization of vasculature between quail and duck, and that the donor NCM may influence this pattern in chimeras. We presume that there are indeed species-specific differences in the pattern of the vasculature given differences in the size and shape of the jaws and specifically, the bony skeleton between quail and duck.

Similarly, our experiments also did not reveal any effects of NCM on the levels of circulating minerals required for osteogenesis. In birds, the calcium that helps mineralize bone comes from the eggshell (Tuan, 1987). In our chimeric system, calcium and inorganic phosphates, which largely comprise apatite crystals, originate from the host blood (Tuan and Nguyen, 1987). Quck maintained levels similar to those observed in control embryos despite their accelerated timetable for mineralization. Thus while NCM initiates and synchronizes each of the steps of bone formation including osteogenic induction, proliferation, differentiation, matrix deposition, and mineralization, the systemic environment appears to be relatively permissive and simply supports osteogenesis independently by providing circulating minerals and a vascular network.

Species-specific differences in cell cycle regulators may underlie beak evolution

At early stages of beak development, the mandibular primordium is largely composed of highly proliferative mesenchyme. However, at the onset of osteogenesis, a subset of these mesenchymal cells take on osteoblast fates, simultaneously decreasing their proliferative capacity and increasing the expression of genes that regulate and encode proteins for bone matrix synthesis (Aubin, 1998; Barlow et al., 1999; Barlow and Francis-West, 1997; Francis-West et al., 1998; Francis-West et al., 1994; McGonnell et al., 1998; Merrill et al., 2008; Stein et al., 1996). At the level of the cell cycle, the transition from proliferation to differentiation is regulated at a checkpoint between the G1 and S phases. G1 arrest allows further differentiation, whereas progression past G1 into S phase allows continued cell cycling and proliferation. This G1-S phase transition is highly regulated by cyclin E (Smith et al., 1997; Smith et al., 1995; Stein et al., 2006; Welcker and Clurman, 2005).

One of the unexpected differences in cell cycle regulation that we observed between species is the expression pattern of cyclin E in the mandible. Quail mandibles consistently showed heavy cyclin E post-translational modification at all stages studied. In contrast, we observed a single dominant cyclin E band in duck samples at all stages examined. This difference holds true and is clear in chimeras where both species-specific states can be observed in the same sample. Given the strong conservation of cyclins among highly disparate taxa (Swenson et al., 1986; Truman et al., 2001), we were surprised by such differences in cyclin regulation within birds. Our data support the possibility that differences in the expression or post-translational processing of even one cell cycle regulator may greatly impact species-specific adaptive evolution. For example, lower levels of functional cyclin E may serve as a mechanism by which species such as quail can dampen mesenchymal proliferation and form a faster-developing, and ultimately, smaller beak.

Our results also suggest that species-specific cell cycle regulation may be linked to size through p27 up-regulation in quail during osteogenic differentiation (versus no apparent change in duck at the same stages), and an earlier decline in cyclin B1. There are numerous studies correlating p27 and size. The most telling involve p27-deficient mice, which are significantly larger than their wild-type littermates, yet with no overt defects in skeletal development (Drissi et al., 1999). Apparently in birds, the developing duck frontonasal process (FNP) has a lower p27 level than in chick, although a possible connection to size has not been discussed previously (Powder et al., 2012). Interestingly, in comparing the single isoform-dominated p27 expression pattern in our mandibular samples to the doublet pattern observed in the FNP, we also characterized what appears to be a tissue-specific post-translational regulation of p27, which has been previously described in other systems (Hirano et al., 2001; Zhang et al., 2005). Thus, modulation of p27 may be a mechanism for tissue-specific increases in size and/or overall growth.

NCM employs Runx2 to control the size of the craniofacial skeleton

In addition to species-specific cell cycle regulation, we also find species-specific regulation of *Runx2*. *Runx2* is often considered a master regulator of osteogenesis since its expression is necessary for bone formation, is sufficient to drive osteoblast differentiation, controls the timing of mineralization, and affects skeletal size (Ducy et al., 1999; Ducy et al., 1997; Eames et al., 2004; Galindo et al., 2005; Komori et al., 1997; Maeno et al., 2011; Otto et al., 1997; Pratap et al., 2003; Thomas et al., 2004). However, a mechanism by which *Runx2* regulates the timing of osteogenesis *in vivo* and also relates to species-specific patterning has not been described previously. Here, by transplanting NCM from faster-developing quail into slower developing duck, we identify *Runx2* as a critical player in both the NCM-dependent timing of osteogenesis, and in the developmental growth and size of the craniofacial skeleton. As osteogenesis proceeds, mandibular *Runx2* levels of the small-beaked quail rise to more than double those of the large-billed duck. By experimentally elevating levels of *Runx2* during development we were able to decrease the size of the beak skeleton, and in effect mirror the relationship between species-specific beak size and endogenous *Runx2* levels. Other studies have also drawn correlations between predicted *Runx2* expression levels and facial length such as in adult dogs and Carnivora (Fondon and Garner, 2004; Sears et al., 2007). Taken together, these data suggest that NCM may be able generate a range of skeletal element sizes and morphologies in part by temporally controlling cell cycle in conjunction with cell differentiation through highly regulated transcription factors such as *Runx2*. Thus, our study offers a functional mechanism in an *in vivo* model that links the regulation of the cell cycle and osteogenesis with *Runx2* expression levels and species-specific skeletal size.

There are many reasons to suspect that NCM controls cell cycle progression and the timing of osteogenesis through tightly interwoven processes. For example, our experiments whereby we over-express D-type cyclins as a means to manipulate cell cycle progression, result in dramatic early up-regulation of *Runx2*. Despite the up-regulation of *Runx2* (and *Col1*), we did not observe any overt morphological phenotype (like asymmetries) in the mandibles at early stages (HH24 and HH27), which we can clearly observe by equivalent stages in quck chimeras and in embryos where we over-express *Runx2*. This indicates that transient cyclin D1/2 overexpression by itself is not sufficient to alter jaw morphology. Nonetheless, we believe the finding that D cyclins when mis-expressed in vivo can affect the expression of an osteogenic differentiation and mineralization factor (i.e., *Runx2*), is significant. Based on this result, we then asked what are the morphological consequences of prematurely over-expressing *Runx2*? Our results show that the timing and levels of *Runx2* have a direct effect on the size of the craniofacial skeleton.

In vitro studies have also shown that *Runx2* can both respond to and modulate cell cycle progression. For example, *Runx2* mRNA and protein levels increase with entry into G1 arrest due to cell density dynamics or serum starvation, but Runx2 can also promote cell cycle exit through direct and indirect mechanisms, including repressing rRNA synthesis, and up-regulating p27 expression (Galindo et al., 2005; Pratap et al., 2003; Thomas et al., 2004; Young et al., 2007). Further, calvarial osteoblasts from *Runx2*-deficient mice have diminished stringency of cell growth control, but this defect can be rescued by re-introduction of exogenous Runx2 (Pratap et al., 2003).

Modularity and plasticity in the osteogenic program promote beak evolution

The implications of our results can be explained through various possible scenarios that would enable NCM to relate cell cycle and the species-specific timing of osteogenesis to the evolution of the craniofacial skeleton. These scenarios involve potential changes to the balance between proliferation and differentiation during a critical phase of osteogenesis, which is condensation. In general, osteogenic condensations are composed of mesenchymal cells, densely packed among a glycoprotein-rich extracellular matrix that facilitates the local signaling necessary for osteoblast differentiation (Ettinger and Doljanski, 1992; Hall, 1980; Hall and Miyake, 1992, 1995). Condensation size, shape, and location are all sources of morphological variation in development and evolution (Atchley and Hall, 1991; Dunlop and Hall, 1995; Hall and Miyake, 2000; Smith and Schneider, 1998; Smith and Hall, 1990). Based on our experiments, we would argue that in absolute time, earlier osteogenic condensations may produce smaller skeletal elements in birds such as quail. In our quck chimeras and in our D-type cyclin gain-of-function experiments, we altered the time course of cell cycle progression, which presumably allowed NCM to reach a critical threshold of condensation sooner and initiate osteogenic differentiation earlier as manifest by premature *Runx2* expression. Such earlier osteoblast commitment would reduce the number of proliferating cells and lead to smaller overall skeletal size. This is also confirmed by our *Runx2* over-expression experiments that reduced beak size.

Likewise, our data further suggest that NCM in species such as duck continues to proliferate more slowly and expand in size for relatively longer periods of time, which ultimately can translate into larger skeletal elements. When comparing quail and duck cell cycle regulation, we find that the quail suppresses proliferative signals, and shows more apparent signs of cell cycle exit. In contrast, the duck supports continued growth along with prolonged differentiation, and achieves a larger overall beak size. An additional scenario is that quail and duck NCM may have intrinsically different responses to signals in adjacent epithelia that affect differentiation and growth. Homologous skeletal condensations between species or condensations from distinct anatomical structures within the same organism (e.g., wing

versus leg), can arise via unique proliferative zones that are established and/or maintained by epithelial signals such as BMPs, FGFs, and SHH (Abzhanov et al., 2006; Abzhanov et al., 2004; Downie and Newman, 1995; Foppiano et al., 2007; Hu and Marcucio, 2009b; Jheon and Schneider, 2009; Schneider, 2007; Shigetani et al., 2002; Sinervo, 2005; Wu et al., 2006; Wu et al., 2004; Young et al., 2010). In all likelihood, each of these scenarios may play a role in providing NCM with the ability to control species-specific size in the craniofacial skeleton.

Overall, our experiments not only reveal that NCM autonomously regulates cell cycle progression and the timing of osteogenic differentiation, but they also indicate that cell cycle and osteogenesis are inexorably linked as a developmental module *in vivo* as they are *in vitro*. The ability of NCM to control and coordinate shifts in timing to both processes, combined with a generally permissive environment provided by surrounding non-NCM derived tissues, such as vasculature, may generate the developmental plasticity necessary for the rapid evolution of beak size and shape. By enabling the osteogenic program to be executed autonomously even in temporally and spatially altered developmental contexts (such as that encountered in the duck or emu host systems) modularity may be an essential element for enhancing the evolvability of the beak (Schneider, 2005). In particular, as part of this highly integrated module, *Runx2* not only appears to function as master regulator of osteoblast differentiation, but also affects the timing of events during osteogenesis, which in turn influences the size of skeletal elements. Moreover, the finding that *Runx2* expression levels are responsive to changes in cell cycle raises the possibility that signaling events surrounding metabolic outcomes relevant to fitness and survival, such as nutrient availability, may influence the rate of growth and morphology of the facial skeleton during development. Finally, the fact that *Runx2* is expressed at species-specific levels that are implemented autonomously by NCM illuminates how NCM may serve as a conduit for generating phenotypic variation during craniofacial evolution.

Acknowledgments

We thank J. Staudinger, N. Grady, T. Heath, D. Hu, E. Berthet, and R. Sklar for technical assistance; R. Marcucio, A. Merrill, J. Fish, C. Mitgutsch, M. Tokita, S. Gline, and A. Goga for helpful discussions. T. Dam at AA Lab Eggs for quail and duck eggs. G. Sheng, K. Ota, and members of the R. Ladher laboratory for assistance with emu eggs. The Q¢PN antibody was obtained from the DSHB maintained by the University of Iowa under the auspices of the NICHD.

FUNDING

Funded in part, by NSF DGE-0648991 to J.H. (J.Y.); NIDCR K99-DE022059 to A.H.J.; NIDCR T32 DE007306 and NIDCR K08 DE021705 to E.L.E.; F32 DE016778 to B.F.E; NIDCR R01 DE019284 to T.A.; and NIDCR R03 DE014795 and R01 DE016402 to R.A.S.

REFERENCES

Abzhanov A, Kuo WP, Hartmann C, Grant BR, Grant PR, Tabin CJ. The calmodulin pathway and evolution of elongated beak morphology in Darwin's finches. Nature. 2006; 442:563–567. [PubMed: 16885984]

Abzhanov A, Protas M, Grant BR, Grant PR, Tabin CJ. Bmp4 and morphological variation of beaks in Darwin's finches. Science. 2004; 305:1462–1465. [PubMed: 15353802]

Atchley WR, Hall BK. A model for development and evolution of complex morphological structures. Biol Rev Camb Philos Soc. 1991; 66:101–157. [PubMed: 1863686]

Aubin JE. Bone stem cells. J Cell Biochem Suppl. 1998; 30-31:73–82. [PubMed: 9893258]

Barlow AJ, Bogardi JP, Ladher R, Francis-West PH. Expression of chick Barx-1 and its differential regulation by FGF-8 and BMP signaling in the maxillary primordia. Developmental Dynamics. 1999; 214:291–302. [PubMed: 10213385]

Barlow AJ, Francis-West PH. Ectopic application of recombinant BMP-2 and BMP-4 can change patterning of developing chick facial primordia. Development. 1997; 124:391–398. [PubMed: 9053315]

Bergers G, Song S. The role of pericytes in blood-vessel formation and maintenance. Neuro Oncol. 2005; 7:452–464. [PubMed: 16212810]

Betsholtz C, Lindblom P, Gerhardt H. Role of pericytes in vascular morphogenesis. EXS. 2005:115–125. [PubMed: 15617474]

Cerny R, Lwigale P, Ericsson R, Meulemans D, Epperlein HH, Bronner-Fraser M. Developmental origins and evolution of jaws: new interpretation of"maxillary" and"mandibular". Dev Biol. 2004; 276:225–236. [PubMed: 15531376]

Chantrain CF, Henriet P, Jodele S, Emonard H, Feron O, Courtoy PJ, DeClerck YA, Marbaix E. Mechanisms of pericyte recruitment in tumour angiogenesis: a new role for metalloproteinases. Eur J Cancer. 2006; 42:310–318. [PubMed: 16406506]

Chen CM, Smith DM, Peters MA, Samson ME, Zitz J, Tabin CJ, Cepko CL. Production and design of more effective avian replication-incompetent retroviral vectors. Developmental biology. 1999; 214:370–384. [PubMed: 10525341]

Coats S, Flanagan WM, Nourse J, Roberts JM. Requirement of p27Kip1 for restriction point control of the fibroblast cell cycle. Science. 1996; 272:877–880. [PubMed: 8629023]

Couly G, Creuzet S, Bennaceur S, Vincent C, Le Douarin NM. Interactions between Hox-negative cephalic neural crest cells and the foregut endoderm in patterning the facial skeleton in the vertebrate head. Development. 2002; 129:1061–1073. [PubMed: 11861488]

Couly GF, Coltey PM, Le Douarin NM. The triple origin of skull in higher vertebrates: a study in quail-chick chimeras. Development. 1993; 117:409–429. [PubMed: 8330517]

Doronkin S, Djagaeva I, Beckendorf SK. The COP9 signalosome promotes degradation of Cyclin E during early Drosophila oogenesis. Dev Cell. 2003; 4:699–710. [PubMed: 12737805]

Downie SA, Newman SA. Different roles for fibronectin in the generation of fore and hind limb precartilage condensations. Dev Biol. 1995; 172:519–530. [PubMed: 8612968]

Drissi H, Hushka D, Aslam F, Nguyen Q, Buffone E, Koff A, van Wijnen A, Lian JB, Stein JL, Stein GS. The cell cycle regulator p27kip1 contributes to growth and differentiation of osteoblasts. Cancer Res. 1999; 59:3705–3711. [PubMed: 10446985]

Ducy P, Starbuck M, Priemel M, Shen J, Pinero G, Geoffroy V, Amling M, Karsenty G. A Cbfa1-dependent genetic pathway controls bone formation beyond embryonic development. Genes Dev. 1999; 13:1025–1036. [PubMed: 10215629]

Ducy P, Zhang R, Geoffroy V, Ridall AL, Karsenty G. Osf2/Cbfa1: a transcriptional activator of osteoblast differentiation. Cell. 1997; 89:747–754. [PubMed: 9182762]

Dunlop LL, Hall BK. Relationships between cellular condensation, preosteoblast formation and epithelial-mesenchymal interactions in initiation of osteogenesis. Int J Dev Biol. 1995; 39:357–371. [PubMed: 7545414]

Ealba EL, Schneider RA. A simple PCR-based strategy for estimating species-specific contributions in chimeras and xenografts. Development. 2013; 140:3062–3068. [PubMed: 23785056]

Eames BF, Schneider RA. Quail-duck chimeras reveal spatiotemporal plasticity in molecular and histogenic programs of cranial feather development. Development. 2005; 132:1499–1509. [PubMed: 15728671]

Eames BF, Schneider RA. The genesis of cartilage size and shape during development and evolution. Development. 2008; 135:3947–3958. [PubMed: 18987028]

Eames BF, Sharpe PT, Helms JA. Hierarchy revealed in the specification of three skeletal fates by Sox9 and Runx2. Dev Biol. 2004; 274:188–200. [PubMed: 15355797]

Ettinger L, Doljanski F. On the generation of form by the continuous interactions between cells and their extracellular matrix. Biol Rev Camb Philos Soc. 1992; 67:459–489. [PubMed: 1463809]

Fondon JW 3rd, Garner HR. Molecular origins of rapid and continuous morphological evolution. Proc Natl Acad Sci U S A. 2004; 101:18058–18063. [PubMed: 15596718]

Foppiano S, Hu D, Marcucio RS. Signaling by bone morphogenetic proteins directs formation of an ectodermal signaling center that regulates craniofacial development. Dev Biol. 2007; 312:103–114. [PubMed: 18028903]

Francis-West P, Ladher R, Barlow A, Graveson A. Signalling interactions during facial development. Mechanisms of Development. 1998; 75:3–28. [PubMed: 9739099]

Francis-West PH, Tatla T, Brickell PM. Expression patterns of the bone morphogenetic protein genes Bmp-4 and Bmp-2 in the developing chick face suggest a role in outgrowth of the primordia. Dev Dyn. 1994; 201:168–178. [PubMed: 7873788]

Galindo M, Pratap J, Young DW, Hovhannisyan H, Im HJ, Choi JY, Lian JB, Stein JL, Stein GS, van Wijnen AJ. The bone-specific expression of Runx2 oscillates during the cell cycle to support a G1-related antiproliferative function in osteoblasts. J Biol Chem. 2005; 280:20274–20285. [PubMed: 15781466]

Gerber H, Vu T, Ryan AM, Kowalski J, Werb Z, Ferrara N. VEGF couples hypertrophic cartilage remodeling, ossification and angiogenesis during endochondral bone formation. Nature Medicine. 1999; 5:623–628.

Hall BK. Tissue interactions and the initiation of osteogenesis and chondrogenesis in the neural crest-derived mandibular skeleton of the embryonic mouse as seen in isolated murine tissues and in recombinations of murine and avian tissues. J Embryol Exp Morphol. 1980; 58:251–264. [PubMed: 7441157]

Hall BK, Miyake T. The membranous skeleton: the role of cell condensations in vertebrate skeletogenesis. Anat Embryol (Berl). 1992; 186:107–124. [PubMed: 1510240]

Hall BK, Miyake T. Divide, accumulate, differentiate: cell condensation in skeletal development revisited. Int J Dev Biol. 1995; 39:881–893. [PubMed: 8901191]

Hall BK, Miyake T. All for one and one for all: condensations and the initiation of skeletal development. Bioessays. 2000; 22:138–147. [PubMed: 10655033]

Hanken J, Wassersug R. The Visible Skeleton: A New double-stain technique reveals the nature of the"hard" tissues. Functional Photography. 1981:22–26. 44.

Hirano K, Hirano M, Zeng Y, Nishimura J, Hara K, Muta K, Nawata H, Kanaide H. Cloning and functional expression of a degradation-resistant novel isoform of p27Kip1. Biochem J. 2001; 353:51–57. [PubMed: 11115398]

Hu D, Marcucio RS. A SHH-responsive signaling center in the forebrain regulates craniofacial morphogenesis via the facial ectoderm. Development. 2009a; 136:107–116. [PubMed: 19036802]

Hu D, Marcucio RS. Unique organization of the frontonasal ectodermal zone in birds and mammals. Dev Biol. 2009b; 325:200–210. [PubMed: 19013147]

Hu D, Marcucio RS. Neural crest cells pattern the surface cephalic ectoderm during FEZ formation. Dev Dyn. 2012; 241:732–740. [PubMed: 22411554]

Hu D, Marcucio RS, Helms JA. A zone of frontonasal ectoderm regulates patterning and growth in the face. Development. 2003; 130:1749–1758. [PubMed: 12642481]

Ishii M, Merrill AE, Chan YS, Gitelman I, Rice DP, Sucov HM, Maxson RE Jr. Msx2 and Twist cooperatively control the development of the neural crest-derived skeletogenic mesenchyme of the murine skull vault. Development. 2003; 130:6131–6142. [PubMed: 14597577]

Jeong J, Mao J, Tenzen T, Kottmann AH, McMahon AP. Hedgehog signaling in the neural crest cells regulates the patterning and growth of facial primordia. Genes Dev. 2004; 18:937–951. [PubMed: 15107405]

Jheon AH, Schneider RA. The cells that fill the bill: neural crest and the evolution of craniofacial development. J Dent Res. 2009; 88:12–21. [PubMed: 19131312]

Komori T, Yagi H, Nomura S, Yamaguchi A, Sasaki K, Deguchi K, Shimizu Y, Bronson RT, Gao YH, Inada M, Sato M, Okamoto R, Kitamura Y, Yoshiki S, Kishimoto T. Targeted disruption of Cbfa1 results in a complete lack of bone formation owing to maturational arrest of osteoblasts. Cell. 1997; 89:755–764. [PubMed: 9182763]

Köntges G, Lumsden A. Rhombencephalic neural crest segmentation is preserved throughout craniofacial ontogeny. Development. 1996; 122:3229–3242. [PubMed: 8898235]

Le Lièvre CS, Le Douarin NM. Mesenchymal derivatives of the neural crest: analysis of chimaeric quail and chick embryos. J Embryol Exp Morphol. 1975; 34:125–154. [PubMed: 1185098]

Liu YH, Tang Z, Kundu RK, Wu L, Luo W, Zhu D, Sangiorgi F, Snead ML, Maxson RE. Msx2 gene dosage influences the number of proliferative osteogenic cells in growth centers of the developing

murine skull: a possible mechanism for MSX2-mediated craniosynostosis in humans. Dev Biol. 1999; 205:260–274. [PubMed: 9917362]

Livak KJ, Schmittgen TD. Analysis of relative gene expression data using real-time quantitative PCR and the 2(-Delta Delta C(T)) Method. Methods. 2001; 25:402–408. [PubMed: 11846609]

Lobjois V, Benazeraf B, Bertrand N, Medevielle F, Pituello F. Specific regulation of cyclins D1 and D2 by FGF and Shh signaling coordinates cell cycle 37 progression, patterning, and differentiation during early steps of spinal cord development. Dev Biol. 2004; 273:195–209. [PubMed: 15328007]

Lwigale PY, Schneider RA. Other chimeras: quail-duck and mouse-chick. Methods Cell Biol. 2008; 87:59–74. [PubMed: 18485291]

Maeno T, Moriishi T, Yoshida CA, Komori H, Kanatani N, Izumi S, Takaoka K, Komori T. Early onset of Runx2 expression caused craniosynostosis, ectopic bone formation, and limb defects. Bone. 2011; 49:673–682. [PubMed: 21807129]

McGonnell IM, Clarke JD, Tickle C. Fate map of the developing chick face: analysis of expansion of facial primordia and establishment of the primary palate. Developmental Dynamics. 1998; 212:102–118. [PubMed: 9603428]

Merrill AE, Eames BF, Weston SJ, Heath T, Schneider RA. Mesenchyme-dependent BMP signaling directs the timing of mandibular osteogenesis. Development. 2008; 135:1223–1234. [PubMed: 18287200]

Mitgutsch C, Wimmer C, Sanchez-Villagra MR, Hahnloser R, Schneider RA. Timing of ossification in duck, quail, and zebra finch: intraspecific variation, heterochronies, and life history evolution. Zoological science. 2011; 28:491–500. [PubMed: 21728797]

Morgan, BA.; Fekete, DM. Manipulating gene expression with replication-competent retroviruse. In: Bronner-Fraser, M., editor. Methods in Avian Embryology. San Diego,: Academic Press; 1996. p. 186-217.

Noden DM. The control of avian cephalic neural crest cytodifferentiationISkeletal and connective tissues. Dev Biol. 1978; 67:296–312. [PubMed: 738529]

Noden DM. Embryonic origins and assembly of blood vessels. Am Rev Respir Dis. 1989; 140:1097–1103. [PubMed: 2478056]

Noden DM. Origins and assembly of avian embryonic blood vessels. Ann N Y Acad Sci. 1990; 588:236–249. [PubMed: 2192642]

Noden DM, Schneider RA. Neural crest cells and the community of plan for craniofacial development: historical debates and current perspectives. Adv Exp Med Biol. 2006; 589:1–23. [PubMed: 17076272]

Otto F, Thornell AP, Crompton T, Denzel A, Gilmour KC, Rosewell IR, Stamp GW, Beddington RS, Mundlos S, Olsen BR, Selby PB, Owen MJ. Cbfa1, a candidate gene for cleidocranial dysplasia syndrome, is essential for osteoblast differentiation and bone development. Cell. 1997; 89:765–771. [PubMed: 9182764]

Pechak DG, Kujawa MJ, Caplan AI. Morphology of bone development and bone remodeling in embryonic chick limbs. Bone. 1986; 7:459–472. [PubMed: 3801237]

Powder KE, Ku YC, Brugmann SA, Veile RA, Renaud NA, Helms JA, Lovett M. A cross-species analysis of microRNAs in the developing avian face. PLoS One. 2012; 7:e35111. [PubMed: 22523571]

Pratap J, Galindo M, Zaidi SK, Vradii D, Bhat BM, Robinson JA, Choi JY, Komori T, Stein JL, Lian JB, Stein GS, van Wijnen AJ. Cell growth regulatory role of Runx2 during proliferative expansion of preosteoblasts. Cancer Res. 2003; 63:5357–5362. [PubMed: 14500368]

Presnell, JK.; Schreibman, MP. Humason's Animal Tissue Techniques. 5th ed. Baltimore: The Johns Hopkins University Press; 1997.

Schneider RA. Neural crest can form cartilages normally derived from mesoderm during development of the avian head skeleton. Dev Biol. 1999; 208:441–455. [PubMed: 10191057]

Schneider RA. Developmental mechanisms facilitating the evolution of bills and quills. J Anat. 2005; 207:563–573. [PubMed: 16313392]

Schneider RA. How to tweak a beak: molecular techniques for studying the evolution of size and shape in Darwin's finches and other birds. Bioessays. 2007; 29:1–6. [PubMed: 17187350]

Schneider RA, Helms JA. The cellular and molecular origins of beak morphology. Science. 2003; 299:565–568. [PubMed: 12543976]

Schneider RA, Hu D, Rubenstein JL, Maden M, Helms JA. Local retinoid signaling coordinates forebrain and facial morphogenesis by maintaining FGF8 and SHH. Development. 2001; 128:2755–2767. [PubMed: 11526081]

Sears KE, Goswami A, Flynn JJ, Niswander LA. The correlated evolution of Runx2 tandem repeats, transcriptional activity, and facial length in carnivora. Evol Dev. 2007; 9:555–565. [PubMed: 17976052]

Shigetani Y, Nobusada Y, Kuratani S. Ectodermally derived FGF8 defines the maxillomandibular region in the early chick embryo: epithelial-mesenchymal interactions in the specification of the craniofacial ectomesenchyme. Dev Biol. 2000; 228:73–85. [PubMed: 11087627]

Shigetani Y, Sugahara F, Kawakami Y, Murakami Y, Hirano S, Kuratani S. Heterotopic shift of epithelial-mesenchymal interactions in vertebrate jaw evolution. Science. 2002; 296:1316–1319. [PubMed: 12016315]

Sinervo B. Darwin's finch beaks, Bmp4, and the developmental origins of novelty. Heredity. 2005; 94:141–142. [PubMed: 15536481]

Smith E, Frenkel B, MacLachlan TK, Giordano A, Stein JL, Lian JB, Stein GS. Post-proliferative cyclin E-associated kinase activity in differentiated osteoblasts: inhibition by proliferating osteoblasts and osteosarcoma cells. J Cell Biochem. 1997; 66:141–152. [PubMed: 9213216]

Smith E, Frenkel B, Schlegel R, Giordano A, Lian JB, Stein JL, Stein GS. Expression of cell cycle regulatory factors in differentiating osteoblasts: postproliferative up-regulation of cyclins B and E. Cancer Res. 1995; 55:5019–5024. [PubMed: 7585545]

Smith KK, Schneider RA. Have gene knockouts caused evolutionary reversals in the mammalian first arch? Bioessays. 1998; 20:245–255. [PubMed: 9631652]

Smith MM, Hall BK. Development and evolutionary origins of vertebrate skeletogenic and odontogenic tissues. Biol Rev Camb Philos Soc. 1990; 65:277–373. [PubMed: 2205303]

Solem RC, Eames BF, Tokita M, Schneider RA. Mesenchymal and mechanical mechanisms of secondary cartilage induction. Dev Biol. 2011; 356:28–39. [PubMed: 21600197]

Stein GS, Lian JB, Stein JL, Van Wijnen AJ, Montecino M. Transcriptional control of osteoblast growth and differentiation. Physiol Rev. 1996; 76:593–629. [PubMed: 8618964]

Stein GS, van Wijnen AJ, Stein JL, Lian JB, Montecino M, Zaidi SK, Braastad C. An architectural perspective of cell-cycle control at the G1/S phase cell-cycle transition. J Cell Physiol. 2006; 209:706–710. [PubMed: 17001681]

Stricker S, Fundele R, Vortkamp A, Mundlos S. Role of Runx genes in chondrocyte differentiation. Dev Biol. 2002; 245:95–108. [PubMed: 11969258]

Swartz M, Eberhart J, Mastick GS, Krull CE. Sparking new frontiers: using in vivo electroporation for genetic manipulations. Dev Biol. 2001; 233:13–21. [PubMed: 11319854]

Swenson KI, Farrell KM, Ruderman JV. The clam embryo protein cyclin A induces entry into M phase and the resumption of meiosis in Xenopus oocytes. Cell. 1986; 47:861–870. [PubMed: 2946420]

Thomas DM, Johnson SA, Sims NA, Trivett MK, Slavin JL, Rubin BP, Waring P, McArthur GA, Walkley CR, Holloway AJ, Diyagama D, Grim JE, Clurman BE, Bowtell DD, Lee JS, Gutierrez GM, Piscopo DM, Carty SA, Hinds PW. Terminal osteoblast differentiation, mediated by runx2 and p27KIP1, is disrupted in osteosarcoma. J Cell Biol. 2004; 167:925–934. [PubMed: 15583032]

Thompson TJ, Owens PD, Wilson DJ. Intramembranous osteogenesis and angiogenesis in the chick embryo. J Anat. 1989; 166:55–65. [PubMed: 2482839]

Tokita M, Schneider RA. Developmental origins of species-specific muscle pattern. Dev Biol. 2009; 331:311–325. [PubMed: 19450573]

Truman, AW.; Kitazono, AA.; Fitz Gerald, JN.; Kron, SJ. Cell Cycle: Regulation by Cyclins, eLS. John Wiley & Sons, Ltd; 2001.

Tuan RS. Mechanism and regulation of calcium transport by the chick embryonic chorioallantoic membrane. J Exp Zool Suppl. 1987; 1:1–13. [PubMed: 2955074]

Tuan RS, Nguyen HQ. Cardiovascular changes in calcium-deficient chick embryos. J Exp Med. 1987; 165:1418–1423. [PubMed: 3572303]

Tucker AS, Lumsden A. Neural crest cells provide species-specific patterning information in the developing branchial skeleton. Evol Dev. 2004; 6:32–40. [PubMed: 15108816]

Wassersug R. A procedure for differential staining of cartilage and bone in whole formalin-fixed vertebrates. Stain Technol. 1976; 51:131–134. [PubMed: 59420]

Wedden SE. Epithelial-mesenchymal interactions in the development of chick facial primordia and the target of retinoid action. Development. 1987; 99:341–351. [PubMed: 3653006]

Welcker M, Clurman B. Cell cycle: how cyclin E got its groove back. Curr Biol. 2005; 15:R810–R812. [PubMed: 16213815]

Wu P, Jiang TX, Shen JY, Widelitz RB, Chuong CM. Morphoregulation of avian beaks: comparative mapping of growth zone activities and morphological evolution. Dev Dyn. 2006; 235:1400–1412. [PubMed: 16586442]

Wu P, Jiang TX, Suksaweang S, Widelitz RB, Chuong CM. Molecular shaping of the beak. Science. 2004; 305:1465–1466. [PubMed: 15353803]

Young DW, Hassan MQ, Pratap J, Galindo M, Zaidi SK, Lee SH, Yang X, Xie R, Javed A, Underwood JM, Furcinitti P, Imbalzano AN, Penman S, Nickerson JA, Montecino MA, Lian JB, Stein JL, van Wijnen AJ, Stein GS. Mitotic occupancy and lineage-specific transcriptional control of rRNA genes by Runx2. Nature. 2007; 445:442–446. [PubMed: 17251981]

Young NM, Chong HJ, Hu D, Hallgrimsson B, Marcucio RS. Quantitative analyses link modulation of sonic hedgehog signaling to continuous variation in facial growth and shape. Development. 2010; 137:3405–3409. [PubMed: 20826528]

Zavitz KH, Zipursky SL. Controlling cell proliferation in differentiating tissues: genetic analysis of negative regulators of G1-->S-phase progression. Curr Opin Cell Biol. 1997; 9:773–781. [PubMed: 9425341]

Zhang W, Bergamaschi D, Jin B, Lu X. Posttranslational modifications of p27kip1 determine its binding specificity to different cyclins and cyclin-dependent kinases in vivo. Blood. 2005; 105:3691–3698. [PubMed: 15665120]

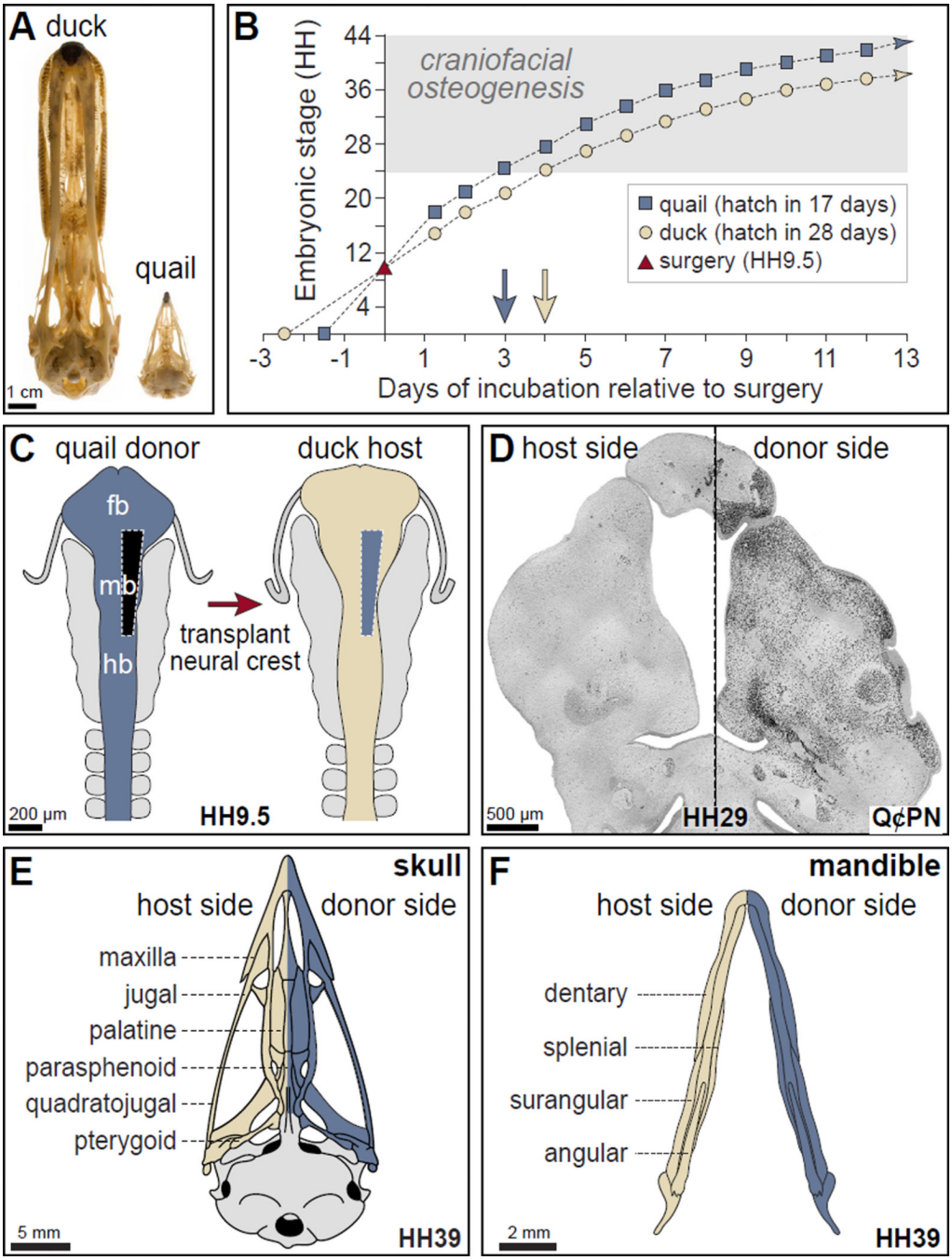

Figure 1. The quail-duck chimeric system

(A) Adult duck and quail skulls demonstrate remarkable species-specific difference in size. **(B)** Embryonic quail (blue squares) and duck (tan circles) have distinct rates of maturation but can be stage-matched at HH9.5 for surgery (red triangle on Y-axis) by setting eggs in the incubator at separate times. Approximately three embryonic stages (HH) distinguish faster-developing quail from duck embryos within two days following surgery, and this three-stage difference remains relatively constant during the period of craniofacial osteogenesis, and represents a separation of approximately 24 hours (blue and beige arrows). **(C)** Schematic of the rostral neural tube at HH9.5 shows the levels of NCM that are grafted unilaterally from

the caudal forebrain (fb), midbrain (mb) and rostral hindbrain (hb) of quail (blue) in place of the same domain in duck (tan). The un-operated side serves as an internal control. **(D)** Coronal section through the mandibular arch of an HH29 chimeric quck (rostral at top). Quail donor NCM (black) are visualized by the quail-specific antibody (Q¢PN) on the surgical (right) side, while few to no quail cells are observed on the contra-lateral duck host side. These cells will give rise to the beak skeleton. **(E)** As shown schematically, quck skulls have a side derived from the duck host as well as a side formed by quail donor NCM. **(F)** The lower beak skeleton of chimeras also contains contributions of donor and host NCM.

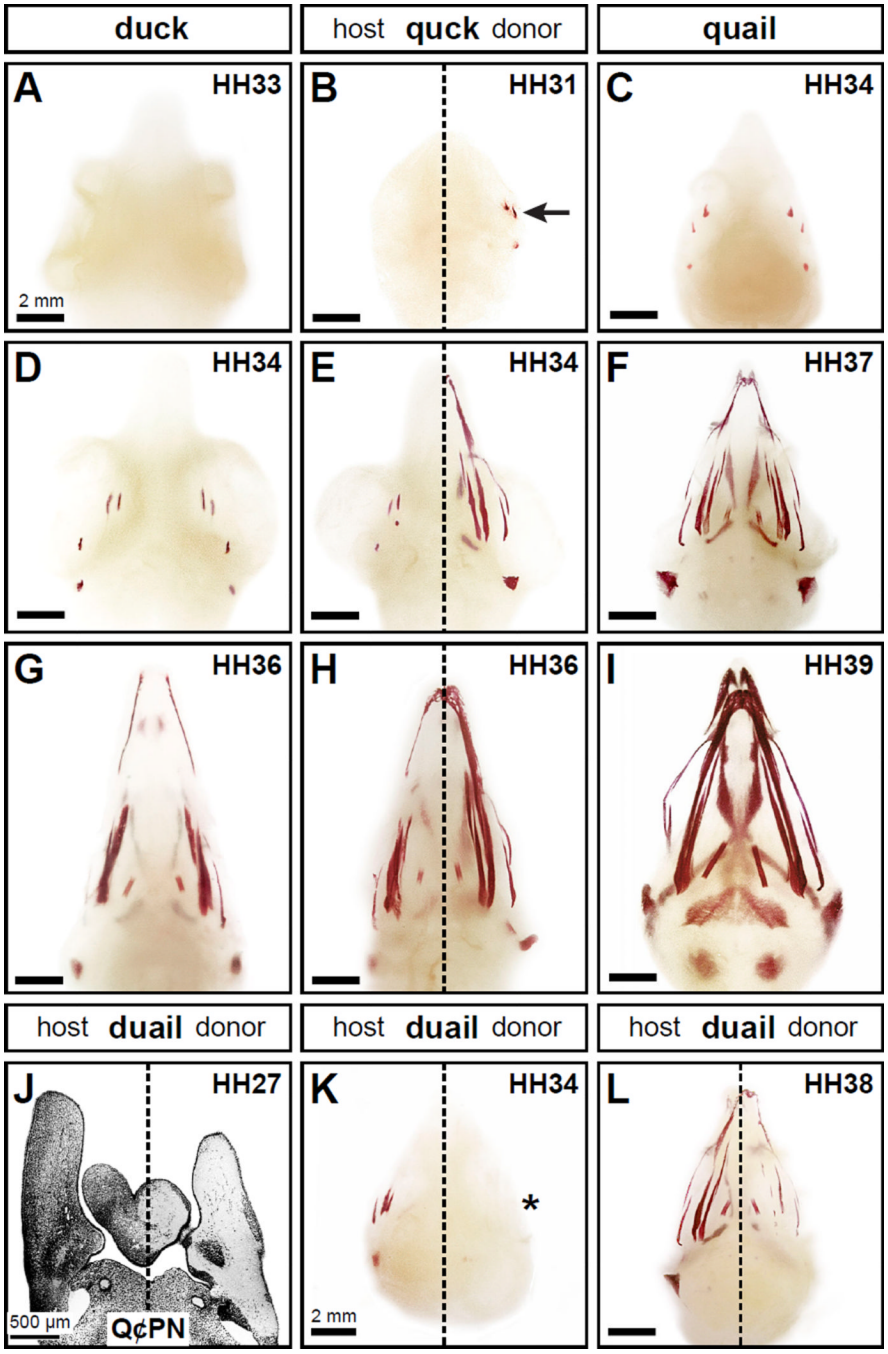

Figure 2. Neural crest mesenchyme controls the timing of mineralization

(A) Neither duck nor quail (not shown) display any signs of mineralization in the head skeleton at HH33 following Alizarin red staining as shown in ventral view. **(B)** In chimeric quck at HH31 (n=4), there is no sign of mineralization on the duck host side but the quail donor side has begun to mineralize (arrow) like that observed in quail three stages later. **(C, D)** Craniofacial mineralization in quail and duck can first be detected at HH34. **(E)** The pattern of mineralization on the quail donor side in quck at HH34 (n=8) is similar to that found in quail at HH37 **(F)** . **(G)** Similarly, mineralization in duck at HH36 is like the host side of quck at HH36 **(H)** whereas the donor side resembles that of quail at HH39 **(I)** (n=8).

(J) In reciprocal transplants that generate chimeric duail, the host side is labeled with Q¢PN-positive quail cells (black) whereas the duck donor side is unlabeled as shown in a coronal section through the mandible at HH27. **(K)** In the heads of chimeric duail stained with Alizarin red, the quail host side follows its normal time course for development and is mineralized at HH34 (n=3). In contrast, on the duck host side mineralization is delayed (asterisk). **(L)** By HH38, the duck donor side of chimeric duail has begun to mineralize (n=3).

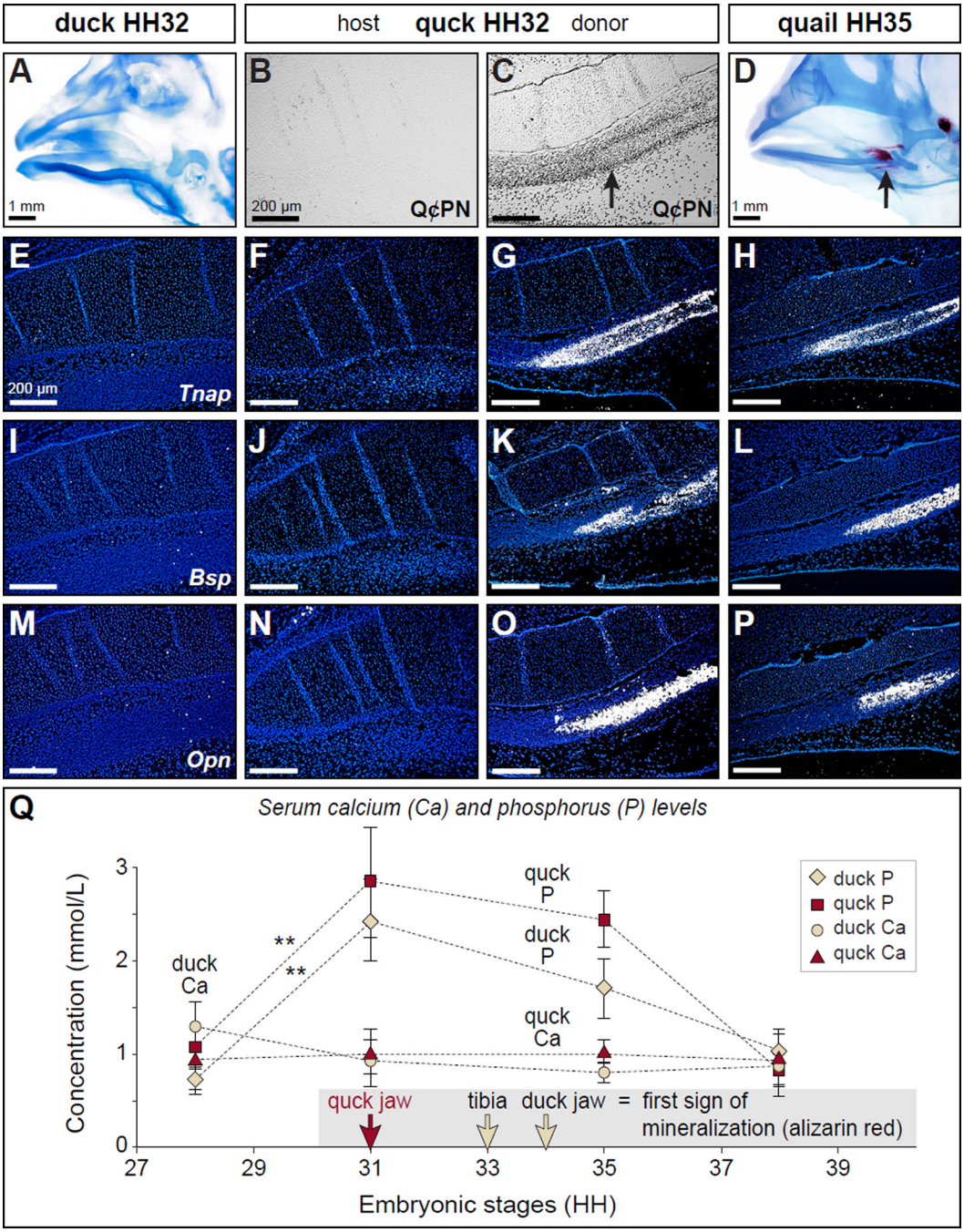

Figure 3. NCM controls the expression of genes involved in mineralization but does not alter host serum mineral levels

(A) At HH32, the beak skeleton of duck and quail (not shown) stains for cartilage (blue) but not bone (red) indicating that mineralization has yet to occur. **(B, C)** Staining sagittal sections of chimeric quck at HH32 shows that the host side is derived from the duck (Q¢PN-negative) whereas the donor side has abundant quail-derived NCM (Q¢PN-positive) especially throughout the angular bone (arrow) in the lower beak skeleton. **(D)** By HH35 mineralization can be detected in the angular bone of quail (arrow) and duck (not shown). **(E-P)** In situ hybridization analyses reveal that molecular markers of mineralization such as *Tnap*, *Bsp*, and *Opn* are not yet expressed in HH32 control duck or on the host side of quck,

whereas high levels of expression on the donor side are coincident with quail donor NCM (Q¢PN-positive) and like that observed in HH35 quail. **(Q)** Serum phosphorous levels increase significantly by HH31 compared to HH28 in both control duck (tan diamond) and quck (red square), preceding the first evidence of mineralization in the beak by at least three stages. Meanwhile, serum calcium levels remain constant throughout the time points studied (HH28-38) in control duck (tan circle) and quck (red triangle). Quantitative data represent the mean ± standard error of the mean (SEM). **, $p \leq 0.01$.

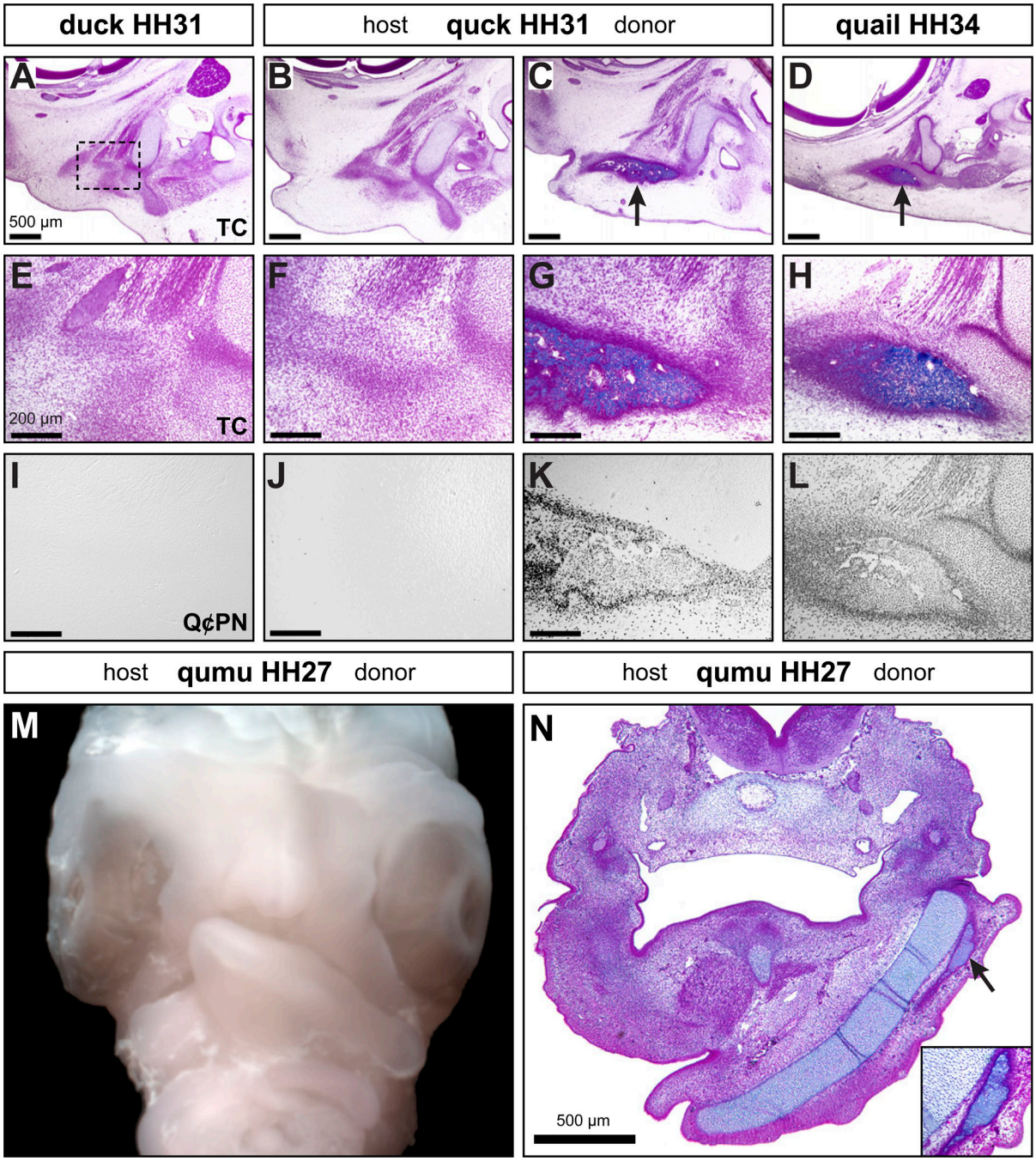

Figure 4. Neural crest mesenchyme controls the timing of osteoid deposition

(A) While osteogenic condensations can be observed (black dashed box indicates region of higher magnification in **(E)**), neither duck nor quail (not shown) have begun to deposit extracellular matrix (osteoid) in the beak skeleton at HH31 as shown in sagittal sections stained with Trichrome (TC). **(B, C)** In quck at HH31, there is no osteoid found on the duck host side but well-developed osteoid on the quail donor side in the surangular bone (arrow). **(D)** The extent of osteoid observed on the quail donor side of quck at HH31 is like that seen in control quail at HH34 (arrow). **(E-H)** Higher magnification views of **(A-D)** demonstrate premature osteoid in quck. **(I-L)** Premature osteoid in quck is coincident with quail donor

NCM (Q¢PN-positive). **(M)** Frontal view of a chimeric qumu head showing asymmetry across the midline as a consequence of differences in the size, shape, and rate of maturation that distinguish the quail donor from the emu host. **(N)** A transverse section through a HH27 qumu reveals a well-developed mandibular cartilage and substantial osteoid deposition on the quail donor side (arrow and inset box), like that observed in control quail seven stages later at HH34.

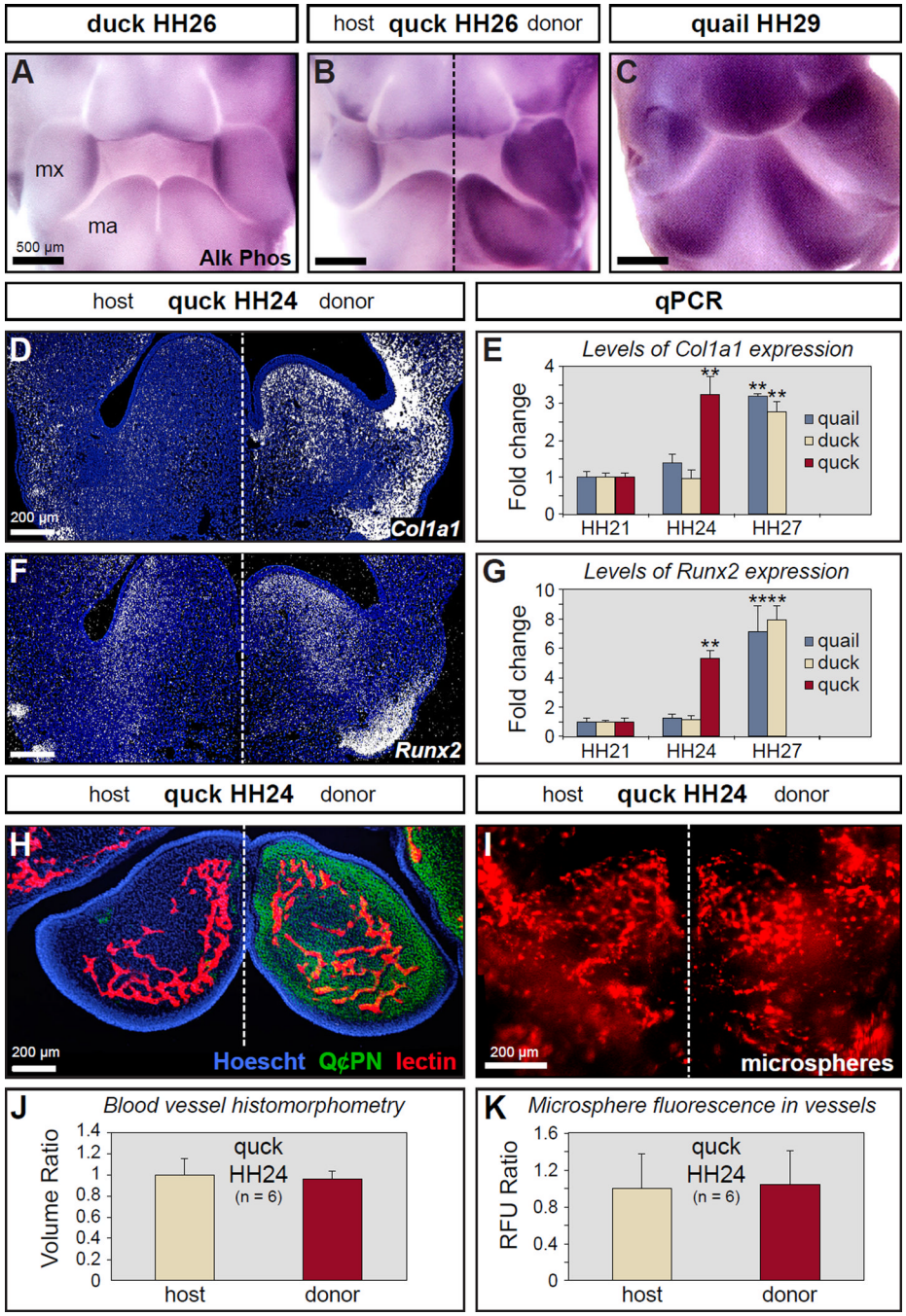

Figure 5. Neural crest mesenchyme controls the timing of osteoblast differentiation

(A) Whole mount assay for alkaline phosphatase activity indicates that there is very little osteoblast differentiation in the mesenchyme of the maxillary (mx) and mandibular (ma) primordia, which form the beak of duck and quail (not shown), at HH26. **(B)** The duck host side of quck at HH26 also shows little evidence of osteoblast differentiation whereas the quail donor side stains darkly like that observed in quail at HH29. **(C)** Quail and duck (not shown) have high levels of alkaline phosphatase activity at HH29 indicating osteoblast differentiation. **(D)** *In situ* hybridization on tissue sections through quck at HH24 shows that *Col1a1* is up-regulated (white signal) on the quail donor side. There is little *Col1a1*

expression in the mandibles of duck and quail at HH24 (not shown). **(E)** RT-qPCR demonstrates that *Col1a1* undergoes a premature 3-fold increase in expression in HH24 quck like that observed in HH27 quail. **(F)** *Runx2* is up-regulated on the quail donor side. **(G)** RT-qPCR shows that *Runx2* undergoes a premature 5-fold increase in expression in HH24 quck like that observed in HH27 quail. **(H)** Tissue section from HH24 quck triple-stained with Hoescht dye (blue) to label all cell nuclei, Q¢PN (green) to label quail donor NCM, and *Lens culinaris* agglutinin (red) to label blood vessels. **(I)** Blood vessels in whole mandibles were visualized by injecting fluorescent microspheres. **(J, K)** Blood vessel volume was quantified and compared between the donor and host sides of quck at HH24 using blood vessel histomorphometry and by measuring fluorescence. Quantitative data represent the mean ± SEM. **, $p \leq 0.01$.

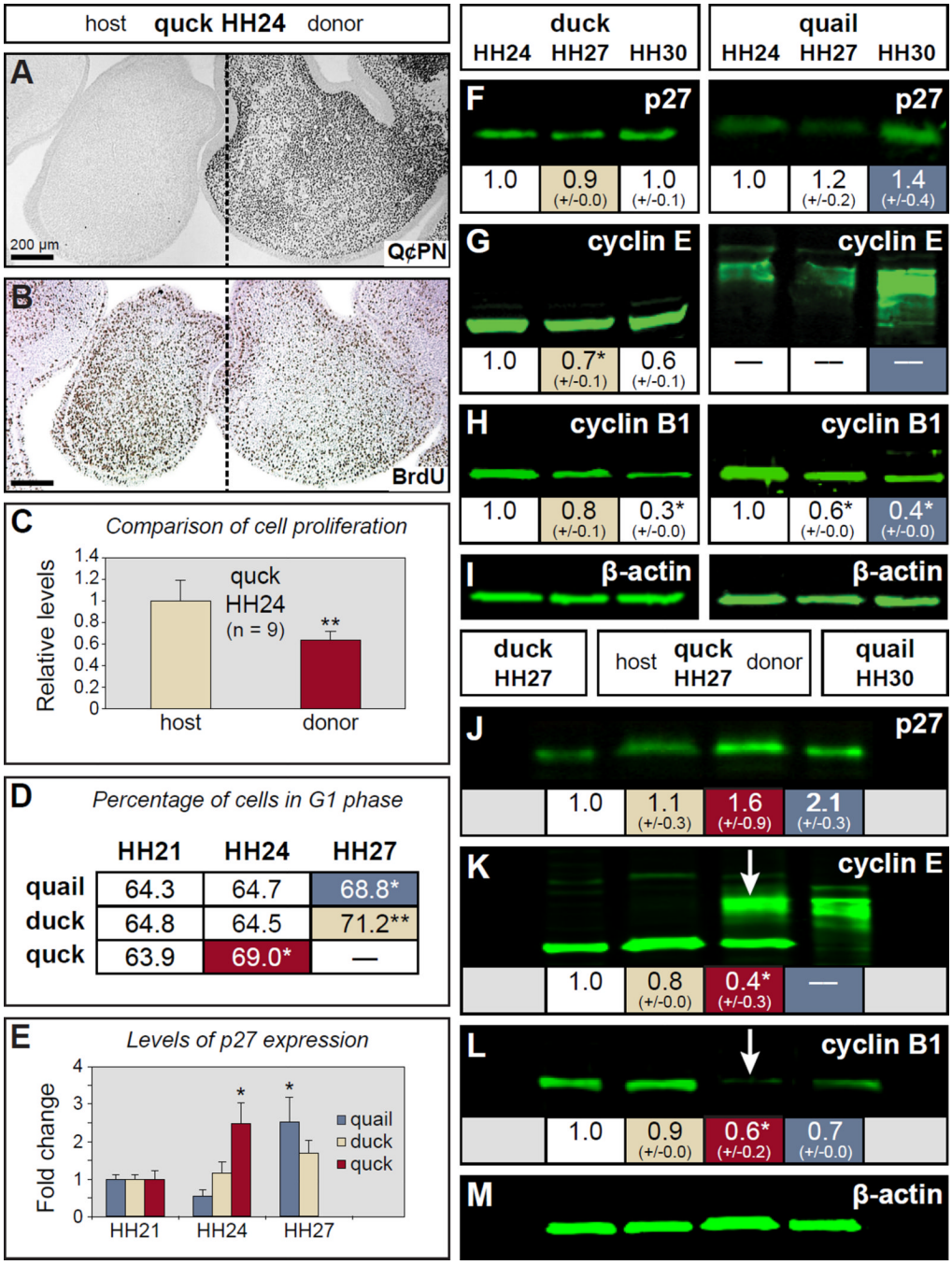

Figure 6. Neural crest mesenchyme regulates cell cycle progression

(A) Section of an HH24 quck showing Q¢PN-positive quail donor NCM (black cells) on one side of the mandible as well as unlabeled duck host tissues. **(B)** An adjacent section stained with an antibody to BrdU (dark brown) showing a decrease in the amount of proliferating cells coincident with the distribution of faster-developing quail donor NCM. **(C)** Quantification of BrdU-positive cells in HH24 quck demonstrates a significant decrease in proliferation on the quail donor side compared to the duck host side. **(D)** At HH24, donor NCM in mandibles from chimeric quck contains a significantly higher percentage of cells in G1 arrest (red-shaded box) versus cells cycling through G2, M, and S phases, which is more

like that observed in quail (blue-shaded box) and duck (beige-shaded box) at HH27, as determined by FACS. **(E)** RT-qPCR reveals that the level of p27 mRNA in quck at HH24 is significantly more like that observed in quail at HH27. For panels **C** , **D** , and **E** , the quantitative data represent the mean ± SEM. *, p≤0.05; **, p≤0.01. **(F-I)** Western blots showing p27, cyclin E, and cyclin B1 expression levels in quail and duck at HH24, HH27, and HH30. β-actin was used as a loading control. **(J-M)** Western blots of host and donor sides of quck at HH27 compared to control HH27 duck and HH30 quail reveal that quail donor NCM express species and stage-specific patterns of protein expression, which can be clearly seen as quail-like for cyclin E **(K,** arrow **)** and cyclin B1 **(L,** arrow **)** on the donor side. For panels **F-M** , the images represent protein levels from a single run of the samples whereas the values shown below are the means of quantified protein levels from multiple runs of the samples ± SEM. * p≤0.05.

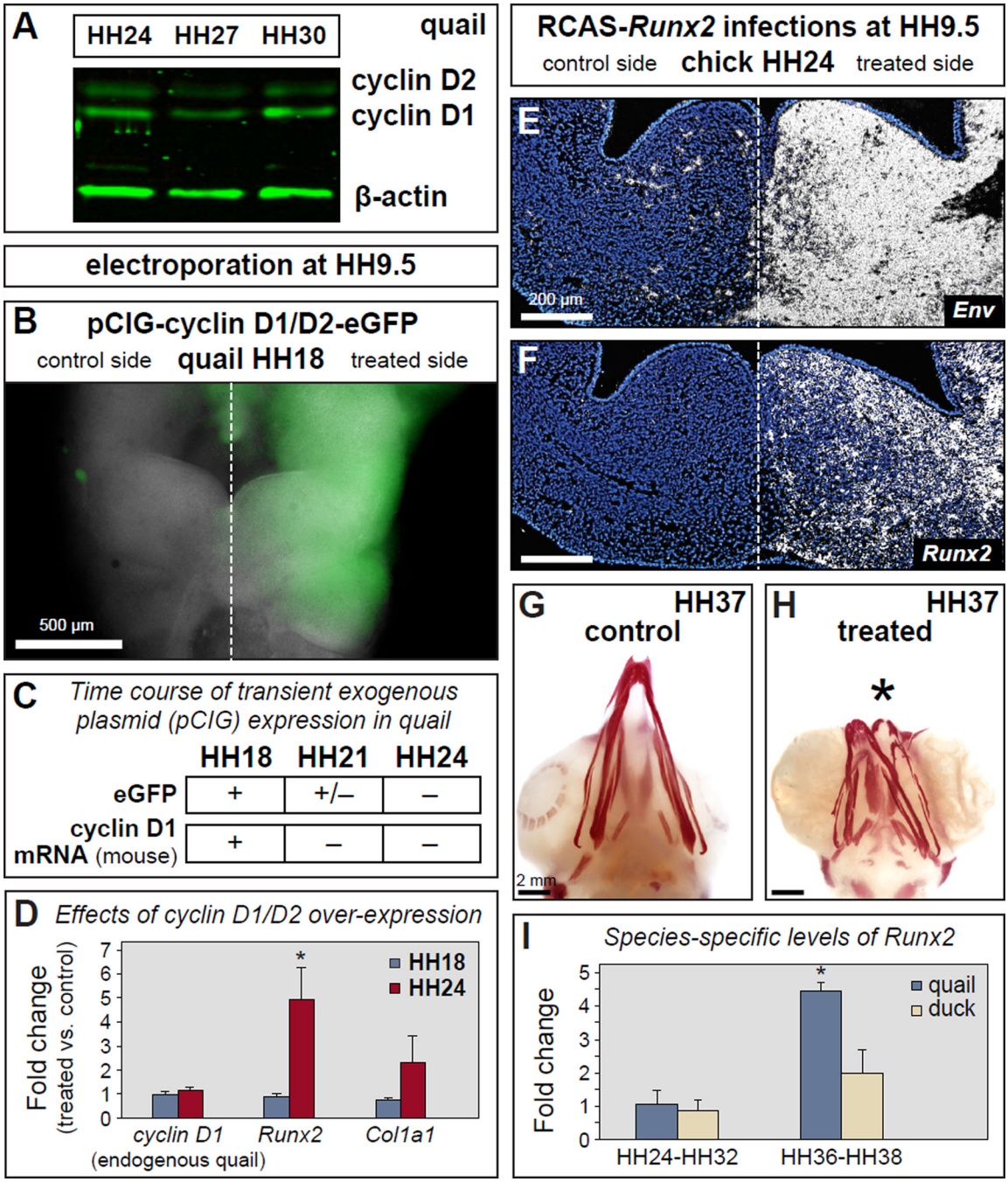

Figure 7. Altering levels of D-type cyclins accelerates *Runx2* expression while premature over-expression of *Runx2* shortens the beak

(A) Endogenous levels of cyclin D1 and D2 in quail mandibles at HH24, HH27, and HH30 as detected by Western blot. **(B)** eGFP (treated side) in quail beak primordia at HH18 indicates overexpression of cyclin D1/D2 following unilateral electroporation of the neural tube at HH9.5 with pCIG-cyclin D1/D2-eGFP. **(C)** Using epifluorescent microscopy, eGFP can be visualized at high levels by HH18, at very low levels by HH21, and not at all by HH24. Loss of plasmid expression is confirmed by RT-qPCR for exogenous (i.e., mouse) cyclin D1 mRNA, which shows transcripts at HH18 but not at HH21 or HH24. **(D)** High levels of exogenous cyclin D1/D2 expression at HH18 do not affect expression of *Runx2* or

Col1a1 when compared to controls. However, the shift from high expression to no expression of exogenous cyclin D1/D2 by HH24 produces a premature 5-fold increase in *Runx2* and an almost 3-fold increase in *Col1a1*. **(E, F)** Injecting RCAS-*Runx2* unilaterally into chick at HH9.5 results in expression of the viral envelope gene (*Env*) and premature overexpression of *Runx2* in the beak primordia as shown by section *in situ* hybridization. **(G)** Control chick infected bilaterally with RCAS-*GFP* show no changes in beak morphology as determined by Alizarin red staining for mineralization. **(H)** Bilateral infections with RCAS-*Runx2* demonstrate that premature overexpression of *Runx2* leads to a drastic shortening of the beak skeleton. **(I)** *Runx2* expression is similar between quail and duck at stages prior to the differentiation of bone in the mandible (HH24-HH32) whereas during matrix deposition and mineralization (HH36-HH38), the differences between *Runx2* levels are significant, with quail more than double that of duck ($p=0.014$). Quantitative data represent the mean ± SEM. *, $p \leq 0.05$.